AD-A084 242 CULLEN COLL OF ENGINEERING HOUSTON TEX F/G 14/2
INTERDISCIPLINARY STUDY ON ADVANCED NDI TECHNIQUES.(U)
JAN 80 A B EL-KAREH, S LONG, C G GARDNER AFOSR-77-3457
UNCLASSIFIED AFOSR -TR-80-0331 NL

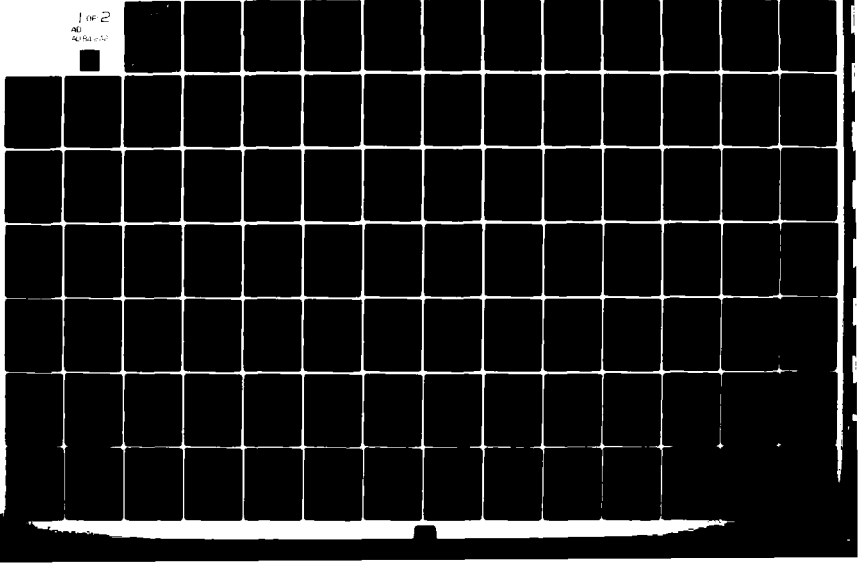

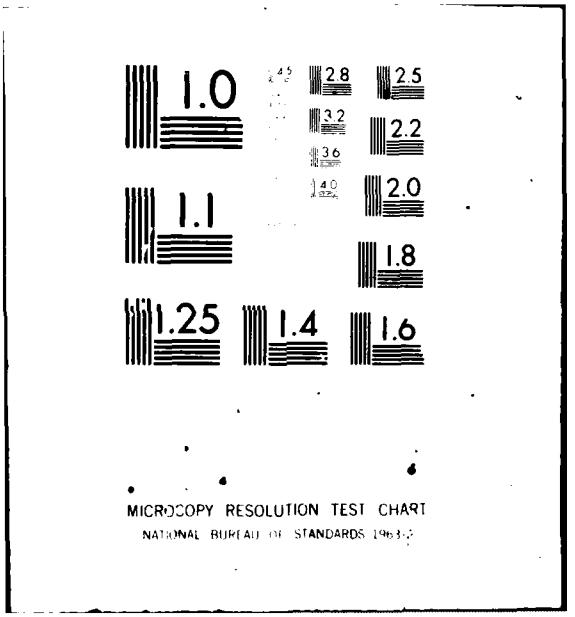
1.0
2.8
2.5
3.2
2.2
3.6
4.0
2.0
1.1
1.8
1.25
1.4
1.6
MICROCOPY RESOLUTION TEST CHART
NATIONAL BUREAU OF STANDARDS 1963-A

LEVEL II

INTERDISCIPLINARY STUDY ON ADVANCED NDI TECHNIQUES

Report for

September 1, 1978 - November 1, 1979

Sponsored by

Air Force Office of Scientific Research

Under a Grant No. AFOSR 77-3457

Prepared by

Auguste B. El-Kareh
C. Gerald Gardner
Stuart Long
Kamal Salama

University of Houston
Cullen College of Engineering
Office of the Dean
Houston, Texas

January 18, 1980

Distribution of this document is unlimited

UNCLASSIFIED
SECURITY CLASSIFICATION OF THIS PAGE (When Data Entered)

(19) REPORT DOCUMENTATION PAGE

READ INSTRUCTIONS BEFORE COMPLETING FORM

1. REPORT NUMBER (18) AFOSR-TR-80-0331	2. GOVT ACCESSION NO. AD-A084 242
3. RECIPIENT'S CATALOG NUMBER (9)	
4. TITLE (and Subtitle) (6) INTERDISCIPLINARY STUDY ON ADVANCED NDI TECHNIQUES	5. TYPE OF REPORT & PERIOD COVERED INTERIM rept. 1 Sep 78 - 30 Nov 79
	6. PERFORMING ORG. REPORT NUMBER
7. AUTHOR(s) A. B. EL-KAREH, K. SALAMA, C. G. GARDNER, STUART LONG (15)	8. CONTRACT OR GRANT NUMBER(s) AFOSR-77-3457
9. PERFORMING ORGANIZATION NAME AND ADDRESS UNIVERSITY OF HOUSTON, CULLEN COLLEGE OF ENGINEERING -202D, HOUSTON, TX 77004 (16)	10. PROGRAM ELEMENT, PROJECT, TASK AREA & WORK UNIT NUMBERS 2307B2, 61102F
11. CONTROLLING OFFICE NAME AND ADDRESS AIR FORCE OFFICE OF SCIENTIFIC RESEARCH/NA, BLDG 410, BOLLING AIR FORCE BASE, D C 20332 (11)	12. REPORT DATE Jan 80
	13. NUMBER OF PAGES 97
14. MONITORING AGENCY NAME & ADDRESS (if different from Controlling Office) (12) 97	15. SECURITY CLASS. (of this report) UNCLASSIFIED
	15a. DECLASSIFICATION/DOWNGRADING SCHEDULE

16. DISTRIBUTION STATEMENT (of this Report)

Approved for public release; distribution unlimited.

17. DISTRIBUTION STATEMENT (of the abstract entered in Block 20, if different from Report)

(10) Augusto B. El-Kareh, Stuart Long, C. Gerald Gardner, Kamal Salama

18. SUPPLEMENTARY NOTES

19. KEY WORDS (Continue on reverse side if necessary and identify by block number)

RESIDUAL STRESSES
MAGNETIC METHODS
EDDY CURRENT TESTING
NONDESTRUCTIVE EVALUATION

20. ABSTRACT (Continue on reverse side if necessary and identify by block number)

Two technical areas are described. Part I: Development of an ultrasonic method for nondestructive evaluation of residual stresses. Part II: Electromagnetic methods for nondestructive evaluation.

*A measure of the temperature dependence of the ultrasonic velocity is used to evaluate the state of internal stress in a solid.

**A study is made on quantitative low frequency eddy current testing on nonferromagnetic structural metals and/or microwave testing of nonmetalic materials.

INTERDISCIPLINARY STUDY

ON ADVANCED NDI TECHNIQUES

AIR FORCE OFFICE
OF
SCIENTIFIC RESEARCH

TABLE OF CONTENTS

TABLE OF CONTENTS

PART II

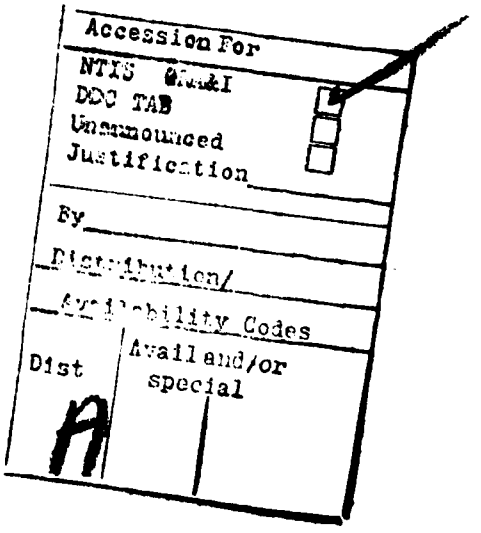

ABSTRACT

This report describes the technical accomplishments during the second year (Phase II) of a research program on the "Development of an Ultrasonic Method for the Nondestructive Evaluation of Residual Stresses." This program has been sponsored by the Air Force Office of Scientific Research under Grant No. AFOSR 77-3457 for research entitled "Interdisciplinary Study on Advanced NDI Techniques." The primary goal of this research program has been the utilization of the temperature dependence of ultrasonic velocity for the nondestructive evaluation of residual stresses in solids. Basically, the temperature dependences of the elastic constants of a solid are due to the anharmonic nature of the crystal lattice, and are directly related to the coefficients of higher-order terms in the strain energy function. A measure of the temperature dependence of the ultrasonic velocity can, therefore, be used to evaluate the state of internal stress in the solid.

During this second year funded for the period 30 September 1978 through 29 September 1979, the sensitivity of the temperature dependence of ultrasonic longitudinal velocity to applied elastic stresses (below yielding) has been studied. The study is performed on two types of commercial aluminum (2024-0 and 6063-T4), and one type of commercial copper (CDA 110). Again, the results of this study show that the velocity changes linearly with temperature, and the slope of the linear relationship decreases linearly as the amount of applied stress is increased within the elastic limit of the specimen under investigation. The maximum decrease in the

temperature dependence in aluminum and copper are respectively 23% which occurred at a stress of 96 MPA, and 6% which occurred at 180 MPA.

The results obtained on aluminum are then used to determine the change as a function of distance of the tangential component of the stresses developed when an aluminum rod is shrunk fit into a slightly smaller eccentric hole drilled in an aluminum disc. Excellent agreement is obtained between the stress distribution determined by the temperature dependence method and that computed using a partial differentiation from a single stress function.

PART I

INTRODUCTION

1. General Considerations

Residual stresses are those contained in a body which has no external traction or other sources of stress, such as thermal gradients or body forces. When the body is externally loaded, these stresses are called internal stresses, and accordingly, residual stresses may be considered as a special case for vanishing external loads. Residual stresses result from non-uniform plastic deformation which includes cold working, forming, forging, heat treatment, etc. Their presence in manufactured components plays an important role in determining the behavior of the component when it is subjected to service loads and environment.

It is important to distinguish between two kinds of residual stresses, namely, the macroscopic stresses which extend over distances of the order of millimeters or greater, and the microscopic stresses which act over short distances and are highly localized from point-to-point[1]. The macroscopic residual stresses vary continuously through the volume of the body and at any point are the combination of the components of stresses in the three principal axes. The microscopic residual stresses (internal stresses) vary greatly from grain to grain and are important to dislocation motion and structure which control many of the material properties. From dislocation theory, it is known that internal stress is proportional to the square root of the dislocation density and is also related to the flow stress of the solid[2,3].

Only in the case of surface stresses in components made of crystalline materials, can nondestructive evaluation of residual

stresses be performed by the X-ray diffraction[4]. Although considerably improved in the last ten years, this method still suffers from serious problems which severely restrict its applications. Ultrasonic methods appear to hold the best promise in measurements of the bulk residual stresses in both crystalline and non-crystalline materials[5]. At present, there are three approaches, namely : dispersion[6], birefringence[7], and harmonic generation[8,9] in which ultrasonic techniques are employed. All these approaches are believed to utilize the anharmonic properties in solids; however, the exact mechanism in each is not yet established.

2. Theoretical Background

Basically, the temperature dependences of the elastic constants are due to the anharmonic nature of the crystal lattice, and can be related to the pressure dependences of these constants. If we consider the isothermal bulk modulus B_T to be a function of pressure and temperature, it follows that[10]

$$\left.\frac{\partial B_T}{\partial P}\right|_T = \frac{1}{\beta B_T}\left[\left.\frac{\partial B_T}{\partial T}\right|_V - \left.\frac{\partial B_T}{\partial T}\right|_P\right], \tag{1}$$

where β is the volume coefficient of thermal expansion. Swenson[11] has show empirically that for many materials

$$\left.\frac{\partial B_T}{\partial T}\right|_V = 0, \tag{2}$$

and it can also be shown by differentiating $(B_S - B_T)$ that

$$\frac{\partial B_S}{\partial P}_T = \left.\frac{\partial B_T}{\partial P}\right|_T \tag{3}$$

to an accuracy of a few percent. Thus it follows that if Swenson's rule is correct,

$$\left.\frac{\partial B_S}{\partial P}\right|_T = \frac{-1}{\beta B_T} \left.\frac{\partial B_T}{\partial T}\right|_P \qquad (4)$$

to an accuracy of a few percent. The right-hand side can be calculated from the measurements of the temperature dependence of the second-order elastic constants. The left-hand side is calculated from the third-order elastic constants C_{ijk}, and equ. (4) is then expressed as[12],

$$\frac{\partial B}{\partial T} = \frac{\beta}{9}\left[C_{111} + 3C_{112} + 3C_{113} + 2C_{123}\right] \qquad (5)$$

More rigorous relationships can be derived[13,14] for the temperature dependence of the longitudinal or the shear modulus which is related to the temperature dependence of the ultrasonic velocity v as,

$$\frac{\partial \ell n M}{\partial T} = 2\frac{\partial \ell n\, v}{\partial T} \qquad (6)$$

From this general argument, it can be seen that the temperature dependence of the ultrasonic velocity (Longitudinal or shear) is a measure of the anharmonic effects generated when the solid is subjected to a stress. A wide range of values for the apparent third order elastic constants were obtained in copper when measurements were made on specimens with different dislocation contributions[10]. Changes in the anharmonic properties due to the presence of internal stresses can therefore be detected by the changes in the slope of the relationship between the ultrasonic velocity and the temperature[15,16]. This slope can be determined with a high accuracy as its value depends only on measurements of the relative changes in the velocity and not on the absolute values.

EXPERIMENTAL APPARATUS AND PROCEDURE

2.1 Specimen Preparation

Commercial aluminum of the types (2024-0 and 6063-T4) and copper of the type (CDA 110) are selected for the present investigation. Specimens were made in the form of rods of 0.95 cm in diameter and 1.29 cm in length, to be suitable for ultrasonic measurements. The two faces of each specimen are then polished to be flat and parallel to within two thousandths of a centimeter over the whole surface.

Some of the specimens, both aluminum type (2024-0) and copper type (CDA 110), were placed in a vacuum furnace for annealing before ultrasonic measurements were undertaken. They were kept in the furnace for four hours at a temperature of 450°C and a pressure of 10^{-6} Torr. This is followed by furnace cooling to provide stress relief to these specimens. The rest of the aluminum type (6063-T4) and the copper type (CDA 110) specimens were employed as received.

2.2 Stress-induced System

The equipment used to apply external stresses on the specimens is shown in Fig. (2.1). It consists of a split collar of inner diameter and height closely equal to those of the specimens used. The collar was made of brass in order to minimize the effect of differences in thermal expansion during the temperature range (280° - 200°K) covered in the temperature dependence measurements. In addition, few drops of high viscosity oil (46500 cs.) was introduced between the screws and the collar, which proved to be effective in keeping the stress applied by tightening the screws of the collar, and simultaneously measuring the change in the diameter of the specimen.

The change in the diameter of the specimen due to the application of stress is measured by means of a shadow-graph purchaesd from Nippon Kogaku K. K. company in Japan. The main principle of the shadow-graph is that the transmittance coefficient is different for different material, and thus the interface between the specimen (aluminum or copper) and the collar (brass) is obviously distinguished. A change in the diameter of the specimen can be visualized and accurately recorded on the screen of shadow-graph with an accuracy of $\pm$ 5%.

BRASS HOLDER

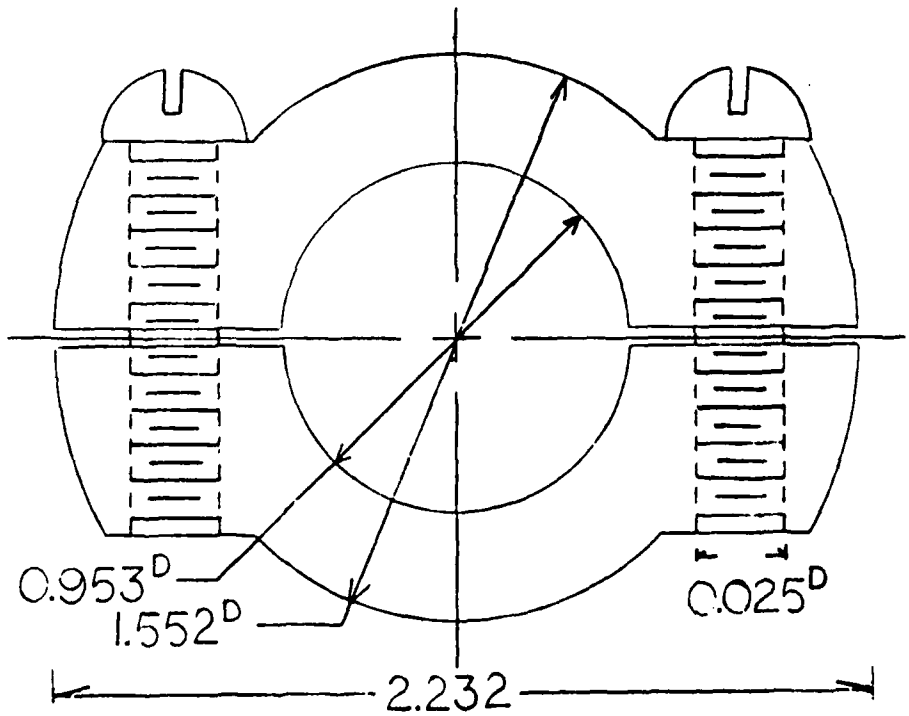

Fig. (2.1) Holder used to apply compressive stress to specimen.

2.3 Pulse Echo Overlap Method and Apparatus

The method utilized in the ultrasonic velocity measurements is the "Pulse Echo Overlap" (P. E. O.) which was originally developed by May (17) and further described by Papadakis (18). In this method, a single transducer acts alternately as a transmitting and receiving transducer. At regular intervals of time, the rf pulsed oscillator imposes a short burst of high-frequency alternating voltage on the transducer which is coupled to the specimen. Through the piezoelectric effect of the quartz transducer, this pulse of alternating voltage converts into a pulse of mechanical vibration having essentially the same frequency as that imposed by the alternating voltage. These stress waves travel through the specimen and return as they encounter a reflecting surface that is perpendicular to the direction of propagation. Upon reaching the transducer through the couplant, the returning pulse causes the transducer to vibrate, and induces an alternating electric voltage which is instantaneously amplified and shown on the oscilloscope.

Fig. (2.2) displays the block diagram of the apparatus used in this investigation. A pulse of approximately 1 μ sec duration of variable pulse-repetition rate is generated by the ultrasonic generator and impressed on a transducer of fundamental frequency 10 MHz which is acoustically bound to the specimen. The reflected

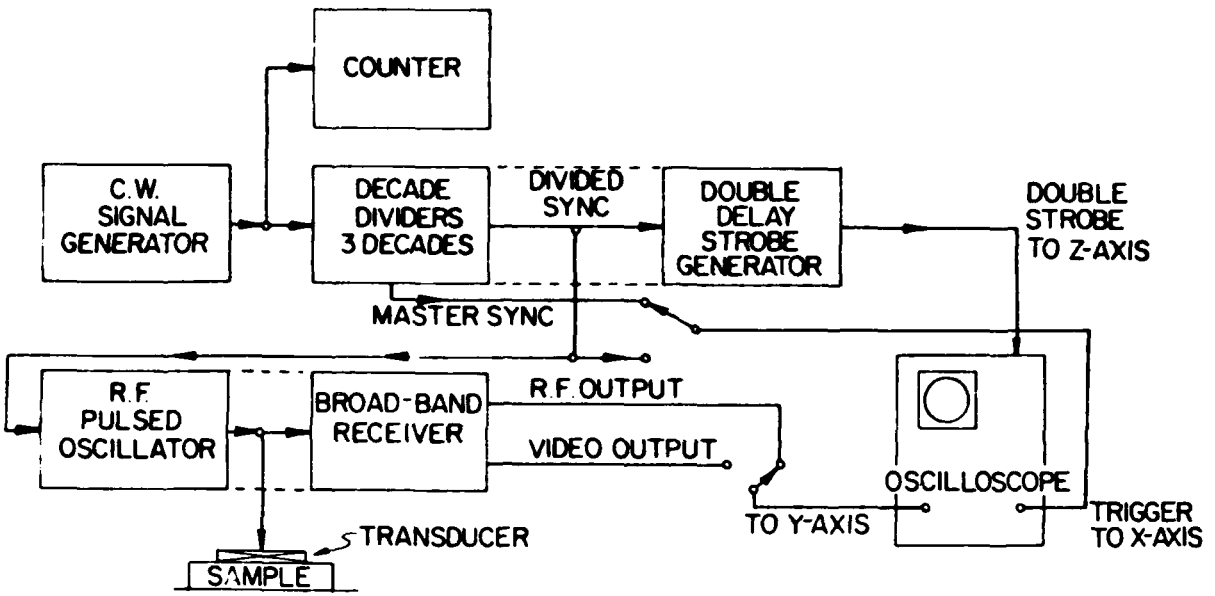

Fig. (2.2) Pulse-echo-overlap system for measuring ultrasonic velocity

rf echoes are received by the same transducer, amplified, detected, filtered, and then displayed on the screen of the oscilloscope. In general, the whole set of instrumentation can be considered as a delay-line technique which means that the delay line produces an exactly overlapped picture of the two 10 MHz modulated echoes only when the triggering frequency rate of the oscilloscope is equal to the riciprocal of the round trip time of the ultrasonic pulse traveling in the specimen. It also means that each delayed time period critically equals the time period between the two echoes, when they are superimposed. This time is determined by the frequency of the pulsed oscillator when the correct cycle-to-cycle match is achieved. This frequency is read on the electronic counter to an accuracy of 1 part in 10^5. The ultrasonic velocity is then calculated using the relationship $V=2lf$, where l is the length of the specimen. X-cut or Y-cut quartz transducers of 0.125 inch diameter and of fundamental frequency 10 MHz are used in this study. The X-cut transducers are used to produce longitudinal (compressional) waves, while Y-cut transducers are used to produce transverse (shear) waves. The transducer is coupled to the test specimen by a thin layer of highly elastic viscous Nonaq stopcock grease.

2.4 Temperature Control System

The temperature control system includes four main parts; namely, cryogenic dewer, vaporization heater, mechanical vacuum pump and potentiometer. All these combinations are to ensure extremely small temperature gradients, high vaccum insulation and very accurate temperature measured over the range between 350 and 4.2°K.

The cryogenic dewer was obtained from the Andonian Cryogenics, Inc., Newtonville, Massachusetts. A diagram of this cooling system is illustrated in Fig. (2.3). During the test, the specimen and the split collar is mounted on the sample-mounting platform (U) and inserted to the sample zone in the dewer. Liquid nitrogen is added directly to the helium reservoir which passes through the capillary tube to the lower end of the sample chamber. The dewer also has a heat exchanger (N) and a thermocouple (V) which provide the adjustment and the measurement of the temperature. Temperature control of the whole system is obtained by establishing a slight excess cooling rate with the throttle valve, and adding just sufficient electrical power to the vaporization heat to bring the sample to the desired temperature level. The potentiometer along with the copper-constantan thermocouple enabled the measurement of the temperature to an accuracy of $\pm$0.1°K.

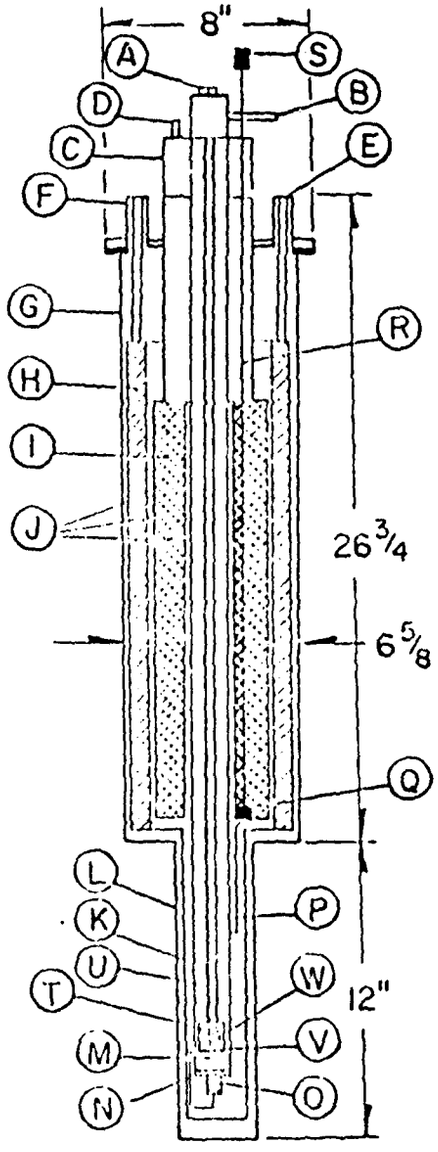

Fig. (2.3) Variable Temperature Cryogenic System Model O-25/7M-250.

LETTER IDENTIFICATION FOR FIGURE (2.3)

A	Electrical Feedthrough
B	Off-Gas Port
C	Top Works
D	Helium Fill & Vent
E	Nitrogen Fill
F	Nitrogen Vent
G	Dewar Body Outer Shell
H	Nitrogen Reservoir
I	Helium Well
J	Vacuum Insulation
K	Nitrogen Temperature Radiation Shield
L	Outer Tail
M	Sample Zone
N	Heat Exchanger
O	Vaporization Heater
P	Capillary
Q	Throttle Valve
R	Throttle Valve Stem
S	Throttle Valve Top Works
T	Sample Temperature Control Heater
U	Sample Holder
V	Cu-Const. Thermocouple
W	Sample

2.5 Measurement Procedure

Several steps are followed to obtain the temperature dependence of the ultrasonic velocity ($\frac{dV}{dT}$). The procedure is as follows:

a) With the specimen properly located in the sample holder, the apparatus (previously described) is adjusted to transmit the rf pulses to the transducer. The reflected echo-train is displayed on the screen of the oscilloscope and two of the echoes are then chosen and overlapped.

b) The sample holder is then placed inside the cryogenic system which is used to maintain the temperature of the specimen at any desired value between 200 and 300°K. Liquid nitrogen is then added to lower the temperature of the specimen.

c) The liquid nitrogen is allowed to flow inside the specimen chamber where the temperature of the specimen is checked by means of the copper-constantan thermocouple attached to the base of the sample holder.

d) After the specimen has been cooled to the desired temperature, no more nitrogen is allowed into the specimen chamber. The voltage of the power supply, connected to the 5 watt resistor (vaporization heater) at the inside bottom of the specimen chamber, is then turned on. The power input is regulated so that a rate of heating of 1 degree per 4 minutes is maintained.

e) The two originally selected echoes are adjusted to overlap on the screen of the oscilloscope and readings of temperature and overlap frequency are recorded. As the temperature of the specimen increases, changes in velocity are directly detected from the phase shift of the two displayed echoes.

f) After approximately fifteen minutes, the two echoes are overlapped again by adjusting the frequency of the C. W. oscillator. The frequency as well as the temperature are then recorded.

g) The previous step is repeated several times as the specimen is allowed to warm up.

h) At any fixed temperature, the velocity is calculated by using the relation,

$$V = 2l f \tag{2.1}$$

where l is the length of the specimen and f is the frequency. When the measurements are made using an X-cut transducer, equation (2.1) gives longitudinal velocities, while transverse velocities are obtained using a Y-cut transducer. The accuracy in measuring changes in the ultrasonic velocity is estimated to be 1 part in 10^5.

i) The data obtained for velocity and temperature are then processed through a computer (IBM 360) to acquire the slope

of this relationship using a least mean square. The computer program used for the determination of the slope is shown in Appendix I.

j) Before another set of velocity measurements are made, the specimen is placed into the brass collar. High viscosity oil (46500 cs.) is put between the screws at the sides of the walls and the collar in order to keep the applied stress uniform and constant during the measurement. The two screws are tightened in order to apply the compressional stress on the specimen. The change in the diameter of the specimen, Δd, is measured by the shadow-graph and the amount of applied stress σ is calculated using the relationship

$$\sigma = -E \times \frac{\Delta d}{d} \qquad (2.2)$$

where E is the Young's modulus and d is the original diameter of the specimen.

k) Steps (a) through (j) are now repeated to obtain a new set of data while the specimen is subjected to the stress. After ultrasonic measurements are finished, the diameter of the specimen is measured again to ensure that the applied stress is within the elastic limit.

l) The specimen is then subjected to a higher stress level, however, within the elastic limit, and a new run is made, following the same procedure.

2.6 Examples of Measurements

Table (2.1) contains typical examples of the results representing the variations of the longitudinal ultrasonic velocity in aluminum as a function of temperature. The experiment is performed while the specimen is subjected to zero stress. The two sets of measurements are made on the same specimen, in order to determine the reproductibility of the values of the temperature dependence. The table includes the values of the longitudinal velocity (Y), measured at temperatures ranging between 180° to 260°K (X). Also included in the table are the recalculated longitudinal velocity (column 3), the deviation (column 4) and the deviation squared (column 5). These quantities are obtained as the computer data output resulting from the least mean square calculations.

The data obtained from the two runs yield values of the best fit for the slope of the temperature dependence of the ultrasonic longitudinal velocity (dV_l/dT). These values are -0.108 and -0.111 in units of m/s.K, for the first and the second run respectively. From these data, one can see that the measurements of the temperature dependence of the ultrasonic velocity can be obtained with an accuracy of $\pm 2\%$. Changes in $\left(\frac{dV}{dT}\right)$ bigger than 2% could be detected and measured.

Table (2.1)

I. First Run

```
GENERAL PURPOSE LEAST SQUARES CURVE FIT
PROGRAM DEVELOPED BY S. CURTICE

C AL SPECIMEN L:1.2871CM 10MHZ 0.250DIA X-CUT STRESS: 0

DEGREE OF POLYNOMIAL ..............   1
NUMBER OF DATA POINTS ..............  20
X-SCALE FACTOR .....................   1.0000
Y-SCALE FACTOR .....................   1.0000
                FIT OF TRANSFORMED FUNCTION
      X              Y          Y-CALCULATED      DEVIATION      DEV. SQUARED
   184.00         6.4060         6.4089         0.28667E-02    0.82182E-05
   188.00         6.4017         6.4046         0.28635E-02    0.82018E-05
   192.00         6.3990         6.4003         0.12608E-02    0.15895E-05
   196.00         6.3953         6.3960         0.65708E-03    0.43176E-06
   200.00         6.3918         6.3917        -0.14591E-03    0.21290E-07
   204.00         6.3874         6.3874        -0.44637E-04    0.22656E-08
   208.00         6.3845         6.3832        -0.14524E-02    0.21094E-05
   212.00         6.3801         6.3787        -0.13552E-02    0.18365E-05
   216.00         6.3767         6.3744        -0.22583E-02    0.50989E-05
   220.00         6.3723         6.3701        -0.21610E-02    0.46700E-05
   224.00         6.3681         6.3656        -0.22640E-02    0.51258E-05
   228.00         6.3636         6.3615        -0.20685E-02    0.42788E-05
   232.00         6.3591         6.3572        -0.18711E-02    0.35010E-05
   236.00         6.3534         6.3522        -0.12274E-02    0.15065E-05
   240.00         6.3455         6.3468        -0.97732E-03    0.76580E-06
   244.00         6.3443         6.3443         0.20022E-04    0.40109E-09
   248.00         6.3389         6.3400         0.12159E-02    0.14785E-05
   252.00         6.3342         6.3357         0.15125E-02    0.22877E-05
   256.00         6.3294         6.3314         0.20103E-02    0.40415E-05
   260.00         6.3239         6.3271         0.32072E-02    0.10286E-04

AVERAGE ABSOLUTE DEVIATION .......    0.15672E-02
AVERAGE SQUARE OF DEVIATION ......    0.32729E-05
AVERAGE PERCENT DEVIATION ........    0.24615E-01
POLYNOMIAL COEFFICIENTS, C(0)...C(1)
   6.6068        -0.10758E-02
```

II. Second Run

```
GENERAL PURPOSE LEAST SQUARES CURVE FIT
PROGRAM DEVELOPED BY S. CURTICE

C AL SPECIMEN L:1.2871CM 10MHZ 0.250DIA X-CUT STRESS: 0

DEGREE OF POLYNOMIAL ..............   1
NUMBER OF DATA POINTS ..............  14
X-SCALE FACTOR .....................   1.0000
Y-SCALE FACTOR .....................   1.0000
                FIT OF TRANSFORMED FUNCTION
      X              Y          Y-CALCULATED      DEVIATION      DEV. SQUARED
   184.00         6.0552         6.0561         0.94414E-03    0.89140E-06
   188.00         6.0512         6.0517         0.49973E-03    0.24973E-06
   192.00         6.0477         6.0473        -0.44346E-03    0.19666E-06
   196.00         6.0437         6.0428        -0.88652E-03    0.78662E-06
   200.00         6.0395         6.0393        -0.24129E-03    0.58216E-07
   204.00         6.0352         6.0339         0.12895E-03    0.16547E-07
   208.00         6.0305         6.0255        -0.10176E-02    0.10354E-05
   212.00         6.0264         6.0250        -0.11618E-02    0.13493E-05
   216.00         6.0204         6.0266         0.19455E-03    0.37850E-07
   220.00         6.0099         6.0117         0.18772E-02    0.35229E-05
   224.00         6.0057         6.0073         0.15640E-02    0.24442E-05
   228.00         6.0024         6.0066         0.41962E-03    0.17608E-06
   232.00         5.9990         5.9984        -0.62376E-03    0.38901E-06
   236.00         5.9952         5.9939        -0.12674E-02    0.16064E-05

AVERAGE ABSOLUTE DEVIATION .......    0.79779E-03
AVERAGE SQUARE OF DEVIATION ......    0.89319E-06
AVERAGE PERCENT DEVIATION ........    0.13263E-01
POLYNOMIAL COEFFICIENTS, C(0)...C(1)
   6.2606        -0.11109E-02
```

RESULTS

3.1 Aluminum

The velocity of longitudinal ultrasonic waves propagating along the axis of the rod was measured as a function of temperature on five aluminum specimens denoted A, B, C, D and E. The measurements were undertaken while the specimens were subjected to various amounts of compressional stresses applied in a plane perpendicular to the direction of propagation of the ultrasonic waves. Typical examples of the results obtained on specimen E are shown in Fig. (3.1), where the longitudinal velocity V_l is plotted vs termperature T, at the stresses 0, 27.6, 46.2 and 75.8 MPa. From these data, one can see that the longitudinal velocity increases linearly with the lowering of temperature, and the slope of this linear relationship between longitudinal velocity and temperature decreases as the applied stress σ is increased. The absolute value of the velocity, however, is increased with the increase of the applied stress, indicating that the specimen becomes stiffer when it is subjected to compressional stresses. The least mean square method was used to determine the slope of the straight line $\frac{dV}{dT}$ which best fits

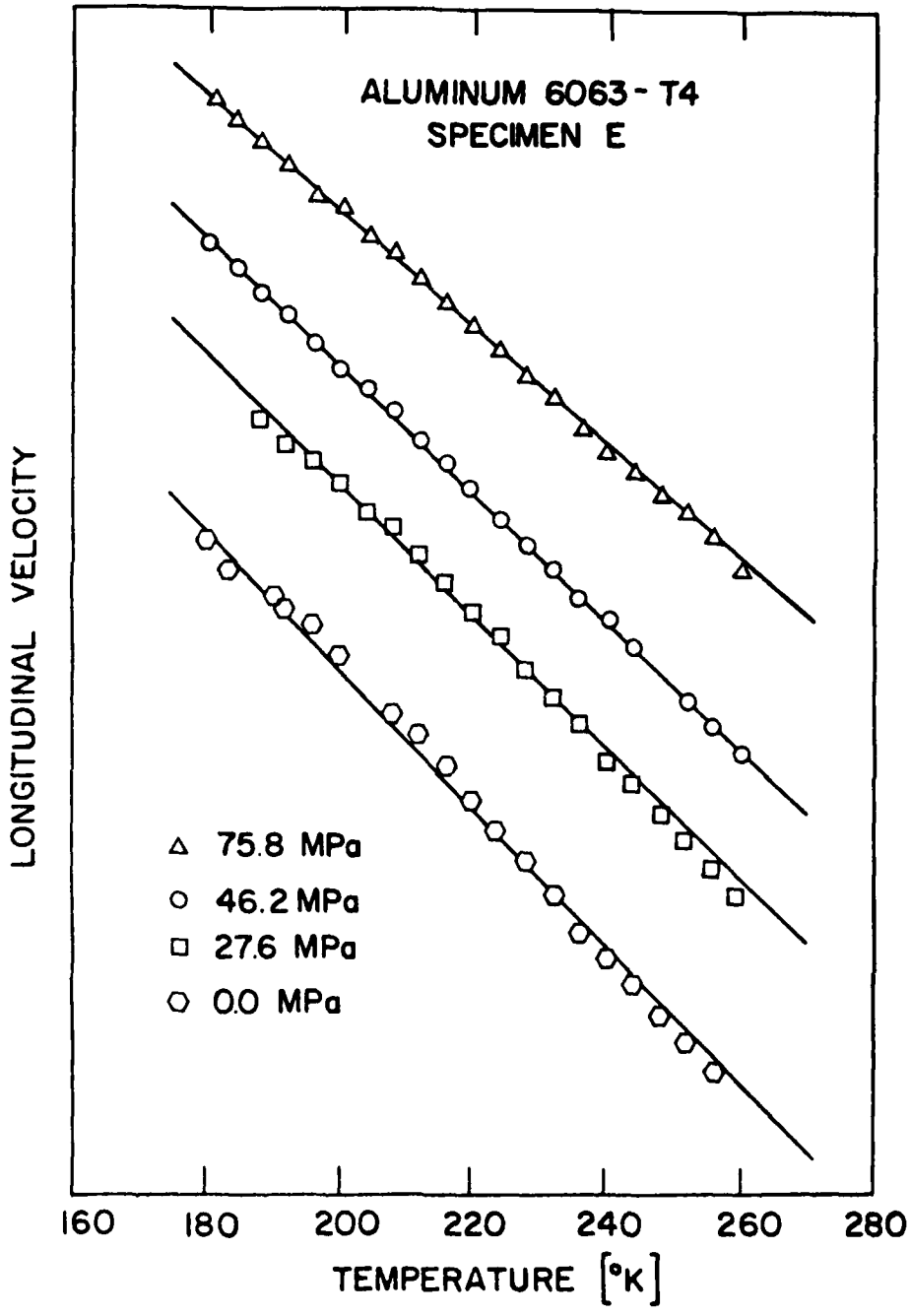

Fig. (3.1) Effect of applied compressive stress on the temperature dependence of ultrasonic longitudinal velocity in aluminum. Stress is applied in a plane perpendicular to the direction of propagation of the ultrasonic waves

the experimental data representing V vs T. The accuracy in determining the temperature dependence of longitudinal velocity by this method is estimated to be $\pm$ 2%.

Table (3.1) lists the results obtained on the five aluminum specimens investigated in this work. The table includes the values of the temperature dependence of the longitudinal velocity, measured at stresses ranging between zero and the yield stress of the specimen. Because the values of the temperature dependence of ultrasonic longitudinal velocity at zero stress were found to vary among specimens investigated, the relative change in the temperature dependence, Δ, due to the application of stress was calculated, and its value are listed in column 4 of Table (3.1). These values of Δ are calculated from the relationship,

$$\Delta = \frac{\left[\frac{dV_\ell}{dT}\right]_o - \left[\frac{dV_\ell}{dT}\right]_\sigma}{\left[\frac{dV_\ell}{dT}\right]_o} \qquad (3.1)$$

The variations in the temperature dependence measured on these specimens at zero stress are believed to be due to the differences in residual stresses in these specimens, even after annealing. Aslo included in this table, is the value of the temperature dependence of the longitudinal velocity at zero stress obtained on annealed pure aluminum (99.999%) (15) which is smaller than any

Table (3.1) Effect of applied compressive stress on the temperature dependence of ultrasonic longitudinal velocity in aluminum. Stress is applied in a plane perpendicular to direction of propagation.

Specimen	Applied Stress (MPa)	$-\frac{dV_\ell}{dT}$ (m/s.K)	Δ %
A (2024-0)	0.0	0.923	0.0
	21.4	0.878	4.9
B (2024-0)	0.0	0.957	0.0
	37.2	0.856	10.6
C (2024-0)	0.0	1.007	0.0
	44.1	0.908	9.8
D (6063-T4)	0.0	1.111	0.0
	94.5	0.866	22.1
E (6063-T4)	0.0	1.066	0.0
	27.6	1.008	5.5
	46.2	0.955	10.4
	75.8	0.875	17.9
Pure, Annealed Ref. (15)	0.0	0.847	

of the temperature dependences measured on these commercial specimens at zero stress.

The results in Table (3.1) indicate that the temperature dependence of longitudinal velocity decreases as the amount of compressional stress is increased. The relative changes in the temperature dependence, obtained on all five specimens investigated, are plotted in Fig. (3.2), as a function of stress applied. The plot shows that all points lie on a straight line which passes through the origin. This indicates that, regardless of the type of aluminum used, the relative change in the measured temperature dependence is a linear function of the applied stress. The slope of this linear relationship is 2.4×10^{-3} per MPa, which yields a maximum change of 23% at a stress of 96 MPa.

The effect of external stress on the temperature dependence of the shear velocity $\frac{dV_s}{dT}$ was investigated in the aluminum specimens D and E. The measurements were performed when the ultrasonic waves were propagated along the axis of the specimen and polarized in the plane in which the stress was applied. Typical examples of the results obtained on specimen E are shown in Fig. (3.3), where the shear velocity V_s is plotted vs temperature T, at stresses 0, 40.7 and 67.0 MPa. Again, the shear velocity increases linearly as the temperature is lowered. However, the slopes of the velocity as a function of temperature remain unchanged as the amount of external stress is changed. The results of the

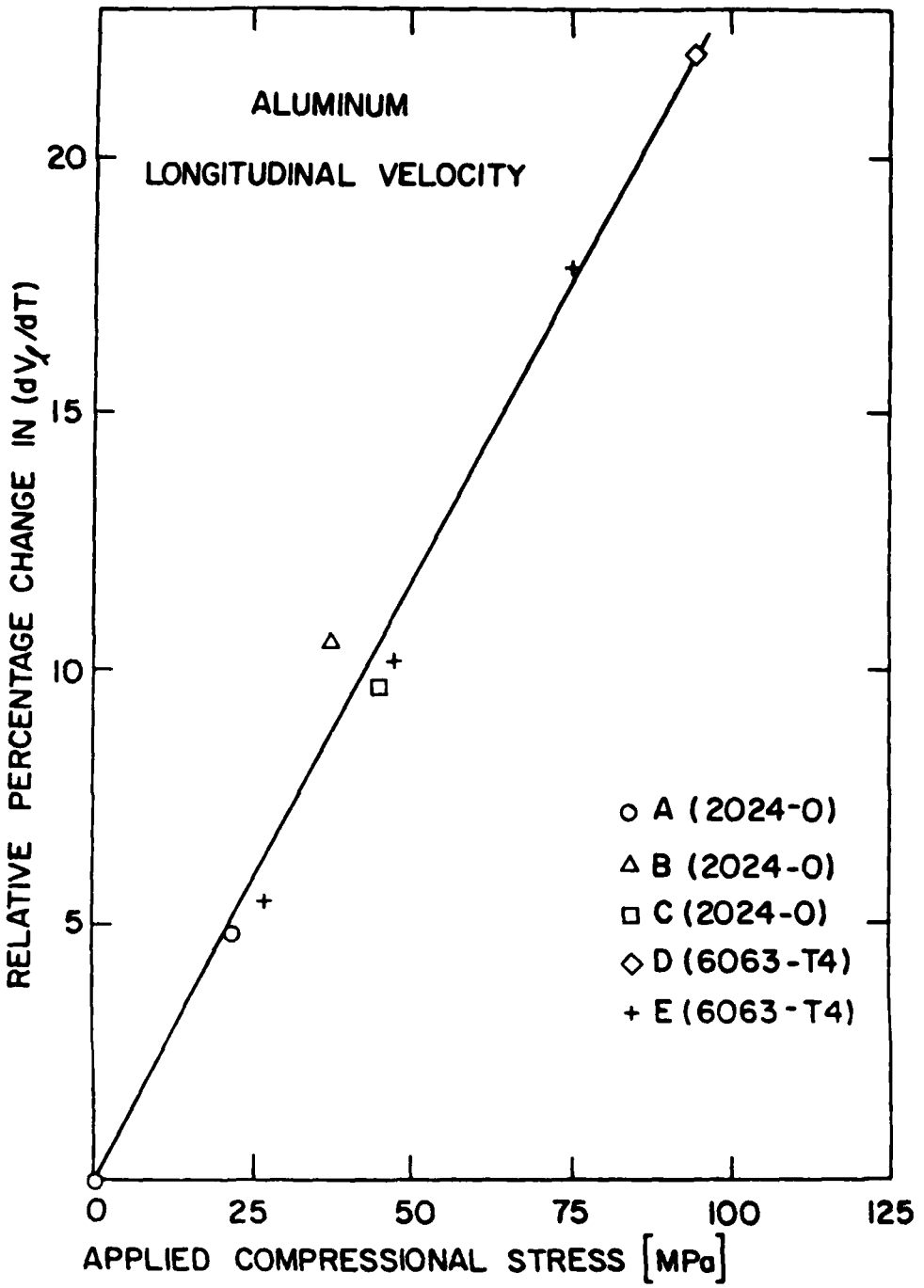

Fig. (3.2) Percentage of the relative change in the temperature dependence of ultrasonic longitudinal velocity as a function of applied stress in aluminum

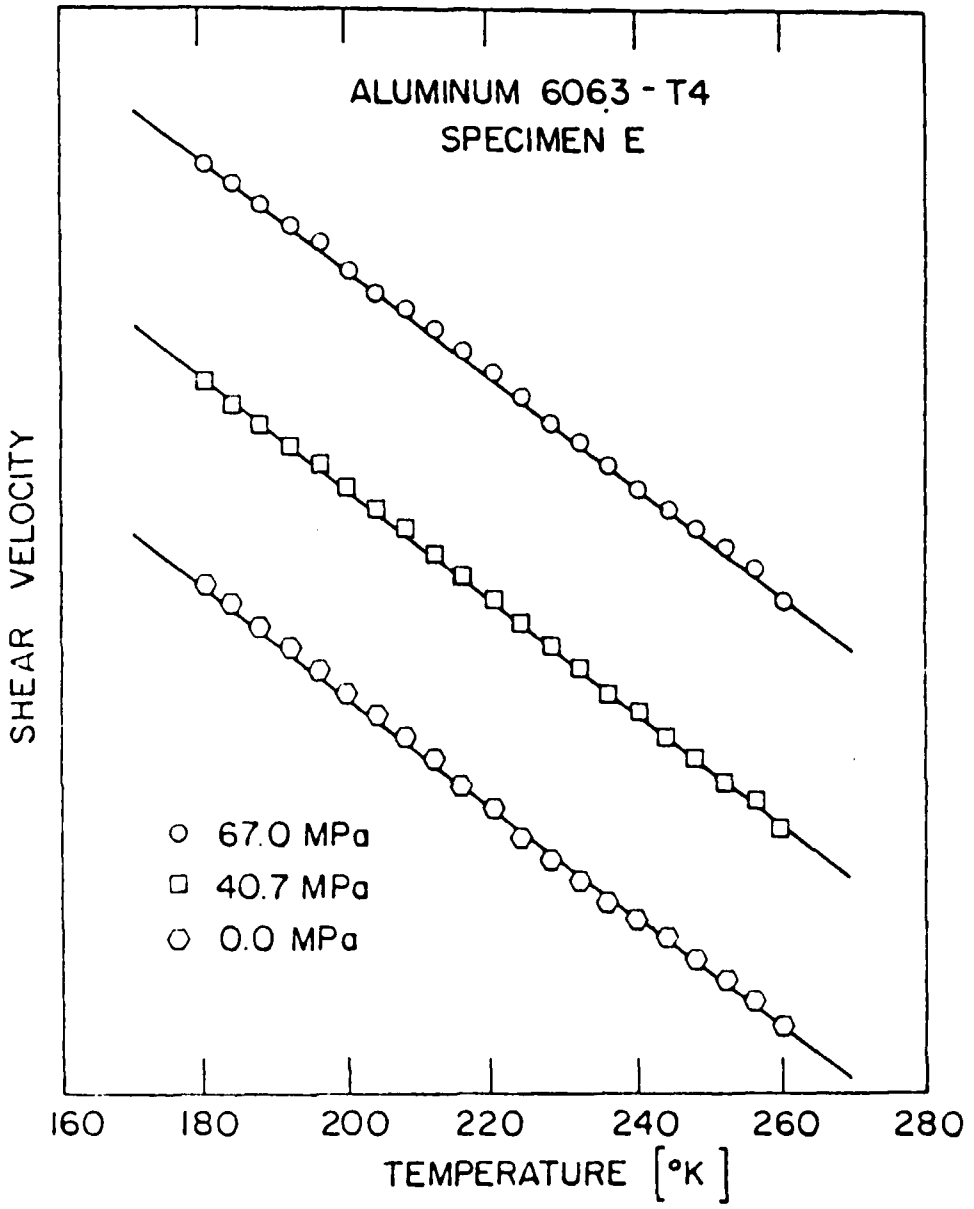

Fig. (3.3) Effect of applied compressive stress on the temperature dependence of ultrasonic shear velocity in aluminum. Stress is applied in a plane perpendicular to the direction of propagation of the ultrasonic waves

measurements obtained on specimens D and E are included in Table (3.2), along with the value of the temperature dependence of shear velocity at zero stress, obtained on pure annealed aluminum, in an earlier study (15). The relative changes in the temperature dependence of the shear velocity, acquired on the two specimens D and E, are plotted in Fig. (3.4), as a function of stress applied. From the results, it is seen that, within the experimental error, $\pm$2%, found in determining the temperature dependence, the temperature dependence of shear velocity in aluminum remains unchanged when external elastic stress is applied in a plane which contains the polarization vector of the ultrasonic waves. This may lead to the conclusion that changes in the temperature dependence of the ultrasonic velocity occur only when the directions of stress and polarization are perpendicular to each other.

Table (3.2) Effect of applied compressive stress on the temperature dependence of ultrasonic shear velocity in aluminum. Stress is applied in a plane perpendicular to the propagation direction.

Specimen	Applied Stress (MPa)	$-\frac{dV_s}{dT}$ (m/s. K)	Δ %
D (6063-T4)	0.0	0.737	0.0
	72.4	0.751	1.9
	96.0	0.758	2.8
E (6063-T4)	0.0	0.767	0.0
	40.7	0.768	0.0
	67.0	0.748	-2.5
Pure, Annealed Ref. (15)	0.0	0.749	

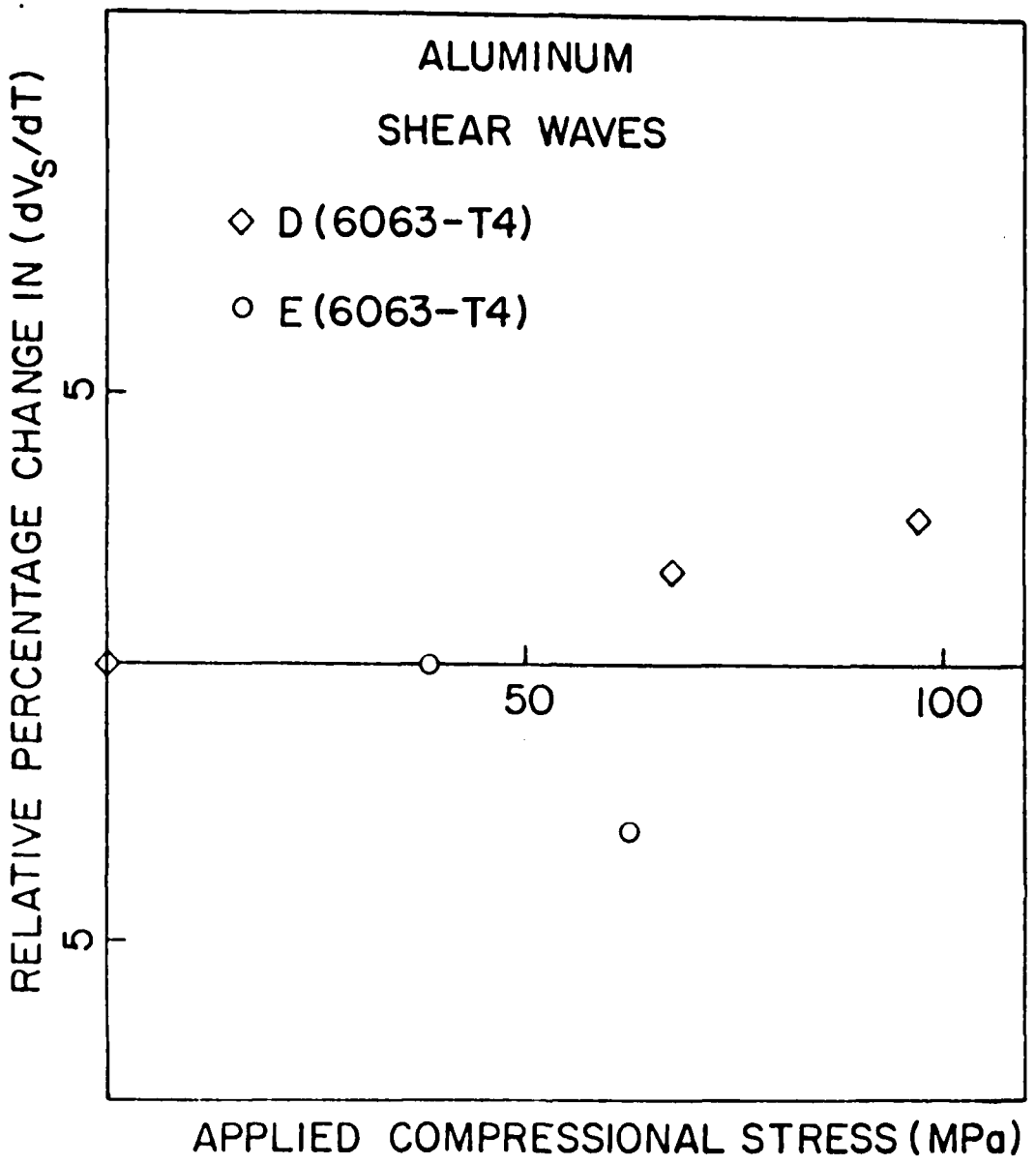

Fig. (3.4) Percentage of the relative change in the temperature dependence of ultrasonic shear velocity as a function of applied stress in aluminum

3.2 Copper

Five copper specimens designated A, B, C, D and E are also investigated in this work. Two of these five specimens were in the annealed state, before any velocity measurements were undertaken, while the other three were used as received. Due to the excessive scattering of the ultrasonic shear waves, only the velocity of longitudinal waves are measured on the copper specimens. This scattering phenomena could be overcome by decreasing the frequency of operation, however,all the present measurements have been made at a frequency of 10 MHz which is the lowest frequency available in the equipment used. Typical examples of the relative changes in longitudinal velocity V_ℓ as a function of temperature T are shown in Fig. (3.5). The measurements are made on specimen C at the stresses 0, 100.7 and 179.9 MPa in the temperature range between 180 and 260°K. From this data, it can be seen that the longitudinal velocity increases linearly with the lowering of temperature, and the slope of this linear relationship between longitudinal velocity and temperature decrease as the applied stress σ is increased. This occurs when the applied stress is within the elastic limit of the specimen.

Table (3.3) contains the results of the temperature dependence of ultrasonic longitudinal velocity obtained on the five copper specimens when they were subjected to external stress applied in a plane perpendicular to the direction of wave propagation. Also

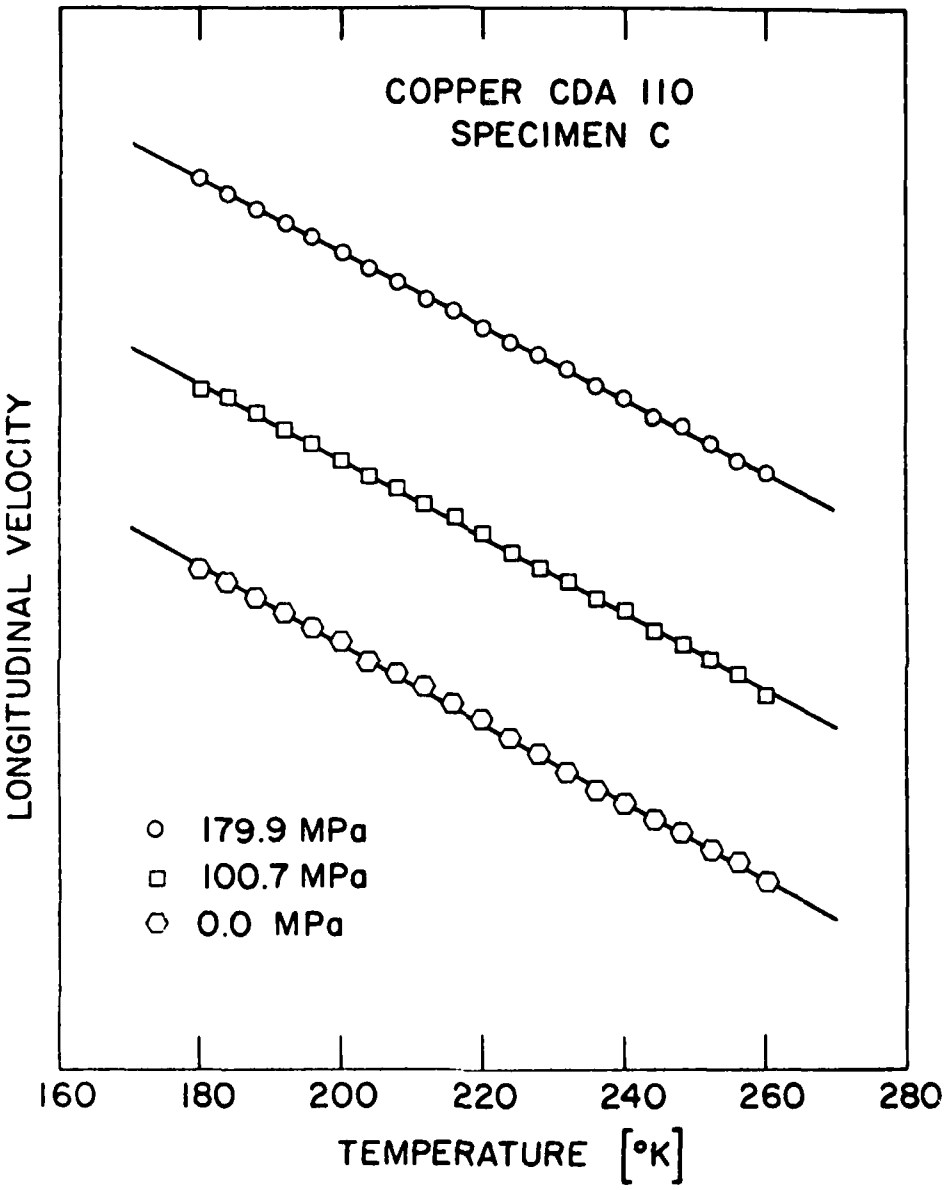

Fig. (3.5) Effect of applied compressive stress on the temperature dependence of ultrasonic longitudinal velocity in copper. Stress is applied in a plane perpendicular to the direction of propagation of the ultrasonic waves

Table (3.3) Effect of applied compressive stress on the temperature dependence of ultrasonic longitudinal velocity in copper. Stress is applied in a plane perpendicular to propagation direction.

Specimen	Applied Stress (MPa)	$-\frac{dV_\ell}{dT}$ (m/s. K)	Δ%
A (CDA 110) Annealed	0.0	0.487	0.0
	23.4	0.484	0.7
	205.4	0.463	4.9
B (CDA 110) Annealed	0.0	0.486	0.0
	117.2	0.468	3.6
C (CDA 110)	0.0	0.557	0.0
	100.7	0.541	2.9
	179.9	0.523	6.1
D (CDA 110)	0.0	0.509	0.0
	59.3	0.502	1.4
	131.0	0.496	2.5
E (CDA 110)	0.0	0.497	0.0
	124.1	0.485	2.9
Pure, Annealed Ref. (16)	0.0	0.495	

included in this table is the value of the temperature dependence of longitudinal velocity at zero stress measured on pure (99.999%) annealed copper (16). In this case the temperature dependence of longitudinal velocity at zero stress is approximately equal to those obtained on commercial annealed specimens, but considerably lower than the temperature dependence determined on the as received specimens.

Similar to the behavior observed in aluminum, the temperature dependence of the ultrasonic longitudinal velocity in copper is found to decrease as the applied stress is increased. The decrease in the temperature dependence for the same stress is, however, much smaller in copper than in aluminum. A plot of the relative change in the temperature dependence of longitudinal velocity as a function of stress for all five copper specimens, is shown in Fig. (3.6). Again, a straight line which passes through the origin, is found to represent the relative changes in the temperature dependence of longitudinal velocity $\frac{dV_\ell}{dT}$ vs stress σ. The maximum value of Δ obtained is about 6% at a stress of 180 MPa. The slope of the straight line is 0.25×10^{-3} per MPa which is approximately an order of magnitude smaller than that calculated from aluminum data.

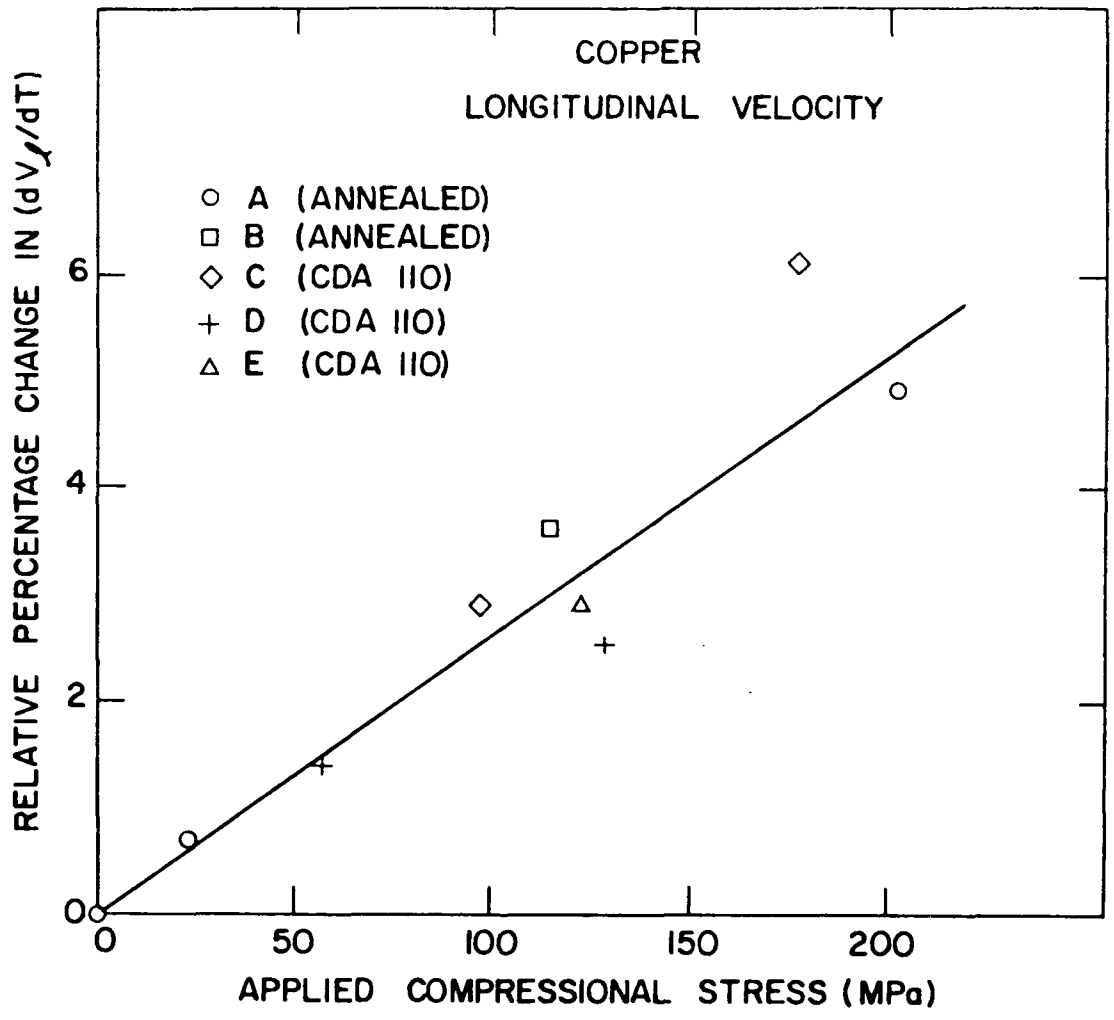

Fig. (3.6) Percentage of the relative change in the temperature dependence of ultrasonic longitudinal velocity as a function of applied stress in copper

DISCUSSION AND APPLICATION

4.1 Discussion of Results

The behavior of the temperature dependence of the ultrasonic velocity as a function of the applied elastic stress for both aluminum Fig. (3.2) and copper Fig. (3.6) suggests that the temperature dependence of the longitudinal ultrasonic velocity measured at an applied compressional stress can be represented by

$$\frac{\left[\frac{dV}{dT}\right]_{\sigma} - \left[\frac{dV}{dT}\right]_{o}}{\left[\frac{dV}{dT}\right]_{o}} = K\sigma \qquad (4.1)$$

where $\left[\frac{dV}{dT}\right]_{o}$ is the temperature dependence at zero stress, and K is a constant equal to 2.4×10^{-3} or 0.25×10^{-3} per MPa for aluminum or copper respectively. Equation (4.1) relates the relative difference of the temperature dependence of the longitudinal velocity with and without stress as a function of the applied stress.

The use of equation (4.1) in the determination of unknown stresses in a specimen, requires the knowledge of the temperature dependence of the ultrasonic velocity at zero stress in the material from which the specimen was made. Theoretical calculations of the value of the temperature dependence of the ultrasonic velocity at

zero stress are not available at present. This means that values of this parameter should be either determined independently by a separate experiment, or estimated from other appropriate results. Measurements of the temperature dependence of ultrasonic velocity at zero stress, made on different types of specimens Table (3.1) and (3.2) have shown that this quantity differs considerably with heat treatment, and to a lesser extent from one specimen to the other. These differences are mainly due to the variations of internal stresses in specimens, even when they are given the same heat treatment. Published data on the changes of the elastic modulii with temperature (including those measured on single crystals) are found to yield temperature dependences which vary considerably among various researchers (19).

Measurements made on the same specimens under simular conditions, have shown that the slope of ultrasonic velocity vs temperature can be determined with an accuracy of $\pm$2%. This quantity along with Fig. (3.2) and Fig. (3.6) yield an accuracy of $\pm$8 MPa and $\pm$25 MPa in determining bulk stresses in aluminum and copper respectively, using the temperature dependence method. These values compare favorably with 14 MPa reported by Smith et al. (20) using a system for acoustoelastic stress analysis which is based on pulse-echo-overlap transit time measurements. They are, however, much larger than those (3.5 MPa) determined by Hsu (21) in his measurements on aluminum plates using the acoustic birefringence method. The accuracy reported by Blinka and Sachse (22) in their

use of interference effects of the out-of-phase polarized waves (0.25 MPa), to determine principal stress differences is of instrument precision and does not describe the accuracy of the method itself.

When the stress applied to the specimen was high enough to cause yielding, the temperature dependence of the longitudinal velocity was found to increase instead of further decreasing. This occured in both aluminum and copper specimens, where the increase in the temperature dependence of longitudinal velocity is increased as long as the stress applied on the specimen was beyond the elastic limits. These results are consistent with those obtained by Salama and Ippolito (23) in their study on the effect of plastic deformation on the temperature dependence of the ultrasonic velocity.

4.2 Determination of Unknown Stresses

In order to examine the possibility of using equation (4.1) to determine unknown stresses, the shrink fit method was employed to introduce known stress distributions in a disc made of type 6063-T4 aluminum. The diameter of the disc was 3.50 cm while its thickness was 0.79 cm. An aluminum rod of the same material was shrunk fit into a hole drilled in the center of the disc. The diameter of the hole was 0.50 cm, while that of the rod was 0.0064 cm larger. In order to fit into the cryogenic system employed to control the temperature of the system, the disc was then machined to its final shape shown in fig. (4.1).

a) Temperature Dependences

The stress generated in the disc due to the presence of the rod can be represented by an axial component σ_a, a radial component σ_r, and a tangential component σ_T, which are related by the relationship, $\sigma_a = \nu(\sigma_r + \sigma_T)$, where ν is the Poisson's ratio. Three independent measurements are undertaken to determine the values of these components: the temperature dependence of the longitudinal and the two shear velocities of ultrasonic waves propagating along the thickness of the disc. The two shear velocities are measured with the polarization vector parallel to and perpendicular to the radial line connecting the center of the rod and the tip of the circumference of the disc. These measurements, evaluate the resultant of the stress components acting in a cylinder of cross-

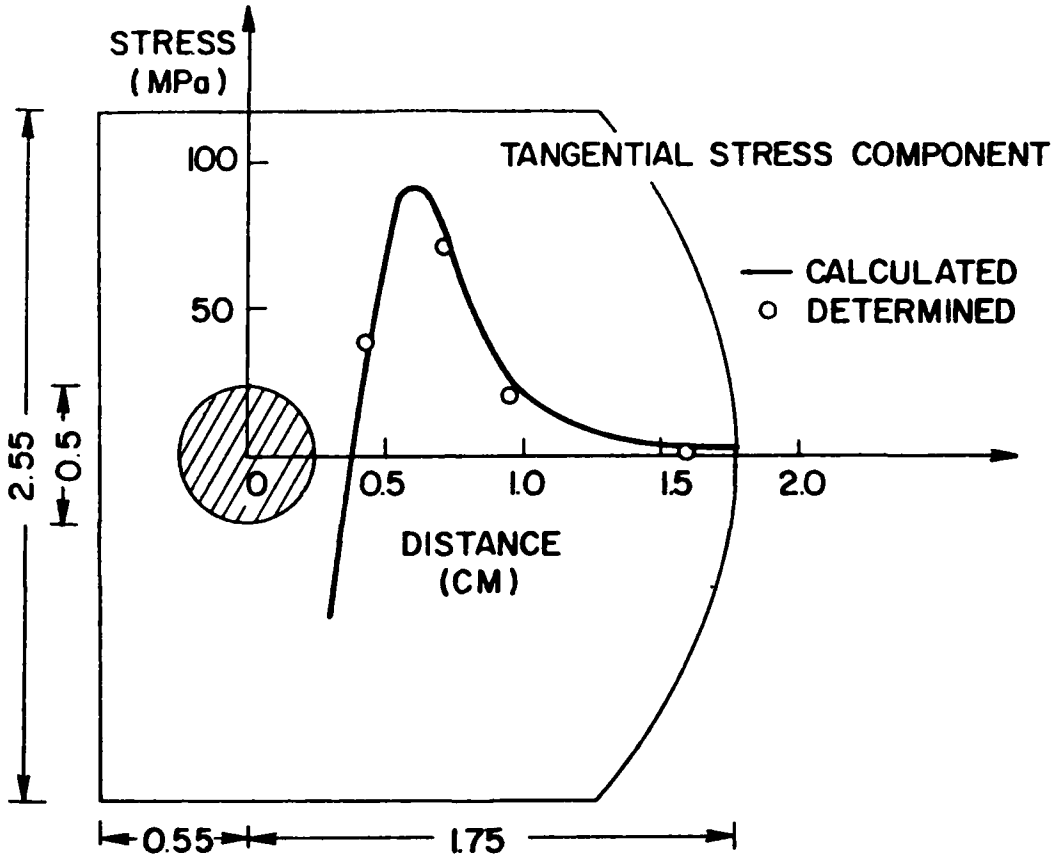

Fig. (4.1) Aluminum disc used for the determination of unknown stresses generated by shrink fit method

sectional area equal to that of the transducer used in the measurements (0.08 cm^2), and of length equal to the thickness of the disc (0.79 cm).

The results of the temperature dependences of the longitudinal and the two shear velocities (dV_ℓ/dT), $(dV_s/dT)_{//}$, and $(dV_s/dT)_\perp$ as a function of distance ranging between 0.45 and 1.60 cm are listed in Table (4.1). These distances are measured between the centers of the rod and the transducers. From this table, one can see that the values of the temperature dependence of longitudinal velocity at the four locations are equal to within +2%. This shows that the stress component measured by the temperature dependence of the longitudinal velocity, remains unchanged over the distance where the measurements were performed. Analysis of stresses in the disc used in the present investigation indicates that only the axial component remains constant over that distance.

The data listed in Table (4.1) also show that the values of the temperature dependences of the two shear velocities obtained at the same distance, are equal to within +1%. This indicates that the stress components measured by these two temperature dependences at the same distance from the center of the rod, should be equal. As a function of distance, however, the values of either of the shear temperature dependences change considerably. Close to the edge of the disc, where the radial or the tangential stress component is expected to be small, the temperature dependence is the largest,

Table (4.1). The temperature dependences of the ultrasonic longitudinal velocity ($\frac{dV_\ell}{dT}$), the ultrasonic shear velocity polarized parallel to the radial direction ($\frac{dV_s}{dT}$)$_{//}$, and the ultrasonic shear velocity polarized perpendicular to the radial direction. ($\frac{dV_s}{dT}$)$_\perp$, as a function of the radial distance R in the aluminum disc shown in Fig. (4.1).

Radial Distance R (cm)	Temperature dependence of ultrasonic velocity (m/s.K)		
	$-(dV_\ell/dT)$	$-(dV_s/dT)_{//}$	$-(dV_s/dT)_\perp$
0.45	1.123	0.821	0.831
0.70	--	0.770	0.756
0.95	1.088	0.868	0.849
1.15	1.113	--	--
1.60	1.107	0.914	0.899

and equal to about -0.9 m/s.K. This value decreases as the distance from the cneter of the rod is decreased, and reaches a minimum around 0.7 cm. As the distance from the rod is further decreased, the value of the temperature dependence of shear velocity is increased again.

b) Calculations of Tangential Stress Component

The stress distribution in the disc shown in Fig. (4.1), can be approximated by that arising in a circular disc with eccentric circular hole shown in Fig. (4.2). This case has been discussed by Jeffery and Filon (24), who showed, that, in the two-dimensional case, the stresses may be derived by the partial differentiation from a single stress function. In the absence of body forces, this stress function χ satisfies the linear partial differential equation of the fourth order,

$$\nabla^4 \chi = 0 \qquad (4.2)$$

where $\nabla^4 = \nabla^2.\nabla^2$, and ∇^2 is the two-dimensional Laplacian $\partial^2/\partial x^2 + \partial^2/\partial y^2$.

Michell (25) gave the general form of the stress-function in polar coordinates, for which the co-ordinate curves are co-axial

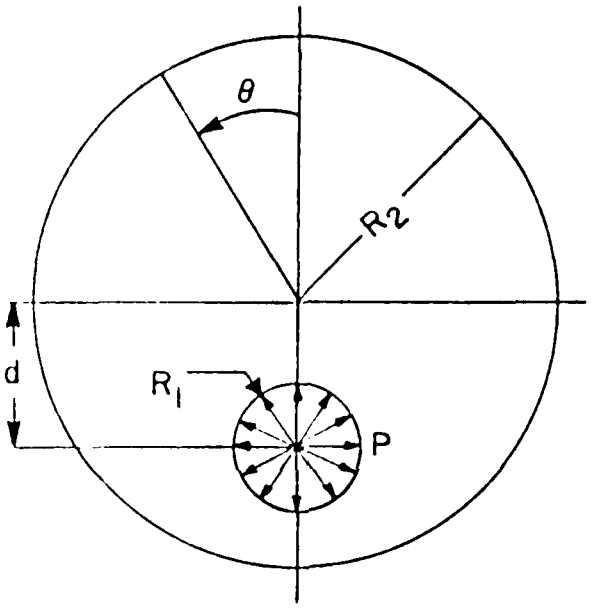

Fig. (4.2) The circular disc with an eccentric hole under inside radial pressure

circles, and thus opened the way for the solution of the problem of a circular disc with an eccentric circular hole. His stress function is expressed as

$$\left(\frac{\partial^4}{\partial\alpha^4} + 2\frac{\partial^4}{\partial\alpha^2\partial\beta^2} + \frac{\partial^4}{\partial\beta^4} - 2\frac{\partial^2}{\partial\alpha^2} + \frac{\partial^2}{\partial\beta^2} + 1\right)(h\chi) = 0 \tag{4.3}$$

where the bipolar coordinates α, β, are defined by

$$\alpha + i\beta = \log\frac{x + i(y + a)}{x + i(y - a)} \tag{4.4}$$

In the above relation, x and y are Cartesian co-ordinates, a is a positive real length, and h is a constant.

Jeffery solved equation (4.3) to obtain the distribution of the tangential stress in a circular disc with an eccentric circular hole (Fig. 4.2), subjected to inside radial pressure P. His solution may be expressed as

$$\sigma_T = 2P\,\frac{R_1^2\left[R_2^2(R_2 - 2d\cos\theta)^2 - (R_1^2 - d^2)^2\right]}{(R_1^2 + R_2^2)\left[R_2^2 - (R_1 + d)^2\right]\left[R_2^2 - R_1 - d)^2\right]} \tag{4.5}$$

where R_1, R_2 are the radii of eccentric circles, d is the distance apart of their centres, θ is the angle counterclockwise from the principle axis. For a rod shrunk fit into the inside circle, P

may be calculated from the relationship (26)

$$P = \frac{\mu R_1 (1 + \nu)}{R_2^2} \epsilon \qquad (4.6)$$

where μ is the shear modulus, ν is the Poisson's ratio, and ϵ is the difference between the diameters of the rod and the inside circle.

Using the dimensions of R_1 and d shown in Fig. (4.1), along with a shear modulus $\mu = 0.26 \times 10^{-5}$ MPa and a Poisson's ratio $\nu = 0.346$, the tangential component of the stress σ_T was calculated as a function of the radial distance. The calculation was made by using equation (4.5), where for $\theta = 0°$, R_2 takes values from 0 to R_2 and for $\theta = 180°$, R_2 takes values from 0 to $(d_1 - R_1)$. The results are plotted in Fig. (4.1). From this plot one can see that the tangential component in this disc is compressive near the rod, equal to zero at approximately 0.4 cm, and becomes tensile at larger distances. Between 0.4 cm and the circumference of the disc, this component has a maximum at 0.6 cm of approximately 95 MPa, which decreases to 1.4 MPa at the circumference. The values of the tangential stress component at the locations where ultrasonic measurements were undertaken, are listed in Table (4.2). Also included in this table, are the values of the temperature dependence of the shear velocity, measured when the polarization vector was perpendicular to the radial direction. At 1.6 cm (close to the

circumference of the disc), $(dV_s/dT)_\perp$ is -0.899 m/s. K and the value of the tangential component is 1.4 MPa. Considering this value of temperature dependence (-0.899 m/s. K) corresponds to the stress calculated at this point (1.4 MPa), the values of the tangential component at the other three locations are calculated using equation (4.1), and the measured values of the temperature dependence at these location. These values are included in column 4 of Table (4.2).

c) Comparison between Experiment and Calculations

From Table (4.2) and Fig. (4.1), one can see that the agreement between the values of the tangential component, and those calculated using Jeffery's equations is very good considering the approximations made in calculating these stresses. The deviation between the calculated stress and that determined from experiment becomes larger at distances close to the eccentric rod. It is probable that this gradual discrepancy is due to the fact that the cross-sectional area of the transducer (0.08 cm^2) used in the measurements determines the average tangential stress components where the slopes of the stress distribution curve change abruptly.

Unfortunately, no comparison could be made between radial stresses determined from the temperature dependence measurements and those calculated from elasticity theory, which are difficult to compute for an eccentric hole in a disc. Nevertheless, the

Table (4.2). Comparison between the calculated values of the tangential stress component and those determined using the experimental values of $(dV_s/dT)_\perp$

Radial Distance R (cm)	$-\left(\frac{dV_s}{dT}\right)_\perp$ (m/s.K)	Applied Stress (Calculated in MPa)	Applied Stress (Measured in MPa)
0.45	0.831	34.0	44.8
0.70	0.756	74.4	69.0
0.95	0.849	22.8	22.1
1.60	0.899	1.4	1.4

values of $(dV_s/dT)_{//}$ listed in Table (4.2), indicate that the distribution of the radial stress component along the axis OX (Fig. 4.1) will be similar to that of the tangential component. At the circumference, σ_r will be equal to zero, increases to a maximum compressive value at R ≃ 0.7 cm, an then drops sharply to zero at R ≃ 0.4 cm. As a function of distance, the sum of the tensile tangential and the compressive radial components $(\sigma_T + \sigma_r)$ should be constant, as indicated from the small variations found in the measurements of the temperature dependence of longitudinal velocity listed in Table (4.2). Values of this quantity determine the axial component of the stress σ_a which is equal to $\nu(\sigma_T + \sigma_r)$. The sum of the tangential and the radial stress components are expected to be small, as the value of (dV_ℓ/dT) listed in Table (4.2) are very close to those measured on specimens D and E of Table (3.1) at zero stress.

REFERENCES

1. Alers, G. A., Proc. Workshop on NDE of Residual Stresses, AFML, NTIAC-76-2, SRI, San Antonio, Texas, 1975.

2. Salama, K. and Roberts, J. M Phys. Stat. Solidi (a) 3, 511 (1970).

3. Salama, K. and Roberts, J. M. Scripta Met. 4, 749 (1970).

4. Residual Stress Measurement by X-Ray Diffraction, SAE J784a, 199, Aug. 1971.

5. Ratcliffe, B. J. Brit. J. Non-Destructive Testing, 11, 48 (1969).

6. Noranha, P. J., Chapman, J. R. and Wert, J. J., J. Testing and Evaluation, 1, 209 (1973).

7. Noranha, P. J., Wert, J. J. and Miser, D. Proc. IEEE Ultrasonic Symposium, 230 (1973).

8. Scorey, C. R., J. Appl. Phys., 41, 2535 (1970).

9. Thompson, R. B., Buck, O. and Thompson, D. O., J. Acous. Soc. Amer., 59, 1087 (1976).

10. Salama, K. and Alers, G. A., Phys. Rev. 161 673 (1967).

11. Swenson, C. A. in Physics of Solids at High Pressures, edited by C. T. Tomizuka and R. M. Emtrick (Academic Press Inc., New York, 1963), p. 548.

12. Thurston, R. N. and Brugger, K. Phys. Rev. 133a, 1604 (1964).

13. Stern, E. A. Phys. Rev. 111, 786 (1958)

14. Garber, J. A. and Granato, A. V. Phys. Rev. 1311, 3990 (1975).

15. Ippolito, R. M. and Salama, K., Proc. 11th Symposium on NDE, P. 62 (1977).

16. Ippolito, R. M. and Salama, K. ISA 24, 403 (1978).

17. May, B. K., IRE National Conv. Rec., 6, pt. 2, 134, 1958.

18. Papadakis, E. P., J. Acoust. Soc. Amer., 42, 1045, 1967.

19. Simmons G. and H. Wang, Single Crystal Elastic Constants and Calculated Aggregate Properties, M. I. T. Press, 1971.

20. Smith, V. D., King, R. R., Cerwin, S. A. Burton, J. R. and McGogney, C. H., National Spring Conf. of Amer. Soc. of NDT, 1975.

21. Hsu, N. N., Exp. Mech., 14, 169, 1974.

22. Blinka, J. and Sachse, W., Exp. Mech. 448, Dec. 1976.

23. Salama, K. and R. M. Ippolito, Proc. First International Symposium on Ultrasonic Materials Characterization, June, 1978.

24. Jeffery, G. B., Plane Stress and Plane Strains in Bipolar Coordinates, Phil. Trans. of Roy. Soc., London, 1921 Series A, Vol. 221, pp. 265-293.

25. Michell, J. H., Proc. London Math. Soc., Vol. 11, p. 100, 1900.

26. Muskhelishvili, N. I., Some Basic Problems of the Mathematical Theory of Elasticity, Wolters-Noordhoff Publishing, Groningen, p. 445, 1963.

PART II

ELECTROMAGNETIC METHODS OF NONDESTRUCTIVE EVALUATION

Principal Investigator

C. Gerald Gardner

Professor

Department of Electrical Engineering

University of Houston, Texas

Stuart A. Long

Associate Professor

Department of Electrical Engineering

University of Houston, Texas

I. Introduction

The general objective of this project is to develop further the rational basis for electromagnetic methods of nondestructive evaluation, particularly in relation to their use as means of quantitatively characterizing performance related properties of structural materials. Attention is presently focused on eddy current methods and microwave methods.

II. Summary of Progress

Progress made to date is briefly summarized below. Further details are presented in Appendices A and B which are the texts of technical papers which have been or are to be submitted for publication in appropriate journals or technical conference proceedings.

A. Eddy Currents

The main effort here has been in modelling mathematically the behavior of an idealized one-turn coil carrying a harmonically time-varying current, in the presence of either a cylindrical conductive core or a planar conductive half-space. Tha aim here is to avoid reliance upon a "brute force" numerical approach, but instead to find approximate analytic solutions from which it is more straightforward to discern both the qualitative and quantitative effects of variations in the important parameters of the situation, e.g., coil radius, frequency of the impressed current, lift-off, and conductivity of the specimen. Although these problems are straightforward to formulate and formally solve as boundary value problems of the vector potential, the resulting formal expressions are formidable integrals, and the usual recourse is to evaluate them numerically for selected values of the associated parameters. We have made an asymptotic expansion of a factor of the integrand (essentially a reflection coefficient) which, while

still requiring numerical evaluation of certain integrals which appear as coefficients, does result in an analytic expression for the coil impedance as a function of the major parameters of the problem. This expression is, however, limited in validity to the case where skin depth is small compared to coil radius or lift-off. Remedies for this restriction are presently being researched.

Another topic being pursued is the calculation of the quantitative effect of discrete flaws (voids of nonconducting inclusions) on the vector potential. Applying the conventional formal theory of scattering we obtain the relation

$$\vec{A}(\vec{r}) - \vec{A}_o(\vec{r}) = j\kappa_o \int_{V_f} \overleftrightarrow{G}_o(\vec{r},\vec{r}') \cdot \vec{A}(\vec{r}')d^3\vec{r}'$$

where $\vec{A}$ is the perturbed vector potential, $\vec{A}_o$ is the unperturbed vector potential (i.e., in the absence of the flaw) $\overleftrightarrow{G}_o(\vec{r},\vec{r}')$ is the (diadic) Green's function for the unperturbed case, κ_o is $\omega\mu_o\sigma$, and V_f is the volume of the flaw. The first step in the solution of this integral equation is to obtain $\overleftrightarrow{G}_o$, which is the Green's function for a harmonically oscillating electric dipole inside the conductive specimen. To the best of our knowledge this problem has not been solved, even approximately, except in special cases (such as at points far from the dipole) not applicable in the present case. We are continuing to work on this problem.

B. Microwave Testing

To this point we have investigated the use of surface electromagnetic waves (SEW) to determine the thickness and dielectric constant of a

dielectric layer supported by a planar conductive substrate. Analysis and experiments at approximately 10 GHz have established the feasibility of this in the case where the dielectric material is "good," i.e., a low-loss material. We consider that the only remaining problem in this area is to extend the results to include dielectric materials with non-negligible losses. (The application would be to structural metals with a thin protective coating of dielectric material.) Also, when extended to higher frequencies (e.g. 100 GHz), it may be possible to detect discrete flaws in such dielectric coatings, and possibly to detect flaws in the conductive substrate.

III. Plans for Future Work

A. Eddy Currents

Significant progress in the theory of eddy current NDE depends upon attaining two objectives, both of which we shall work toward. First, a better method of analytically approximating the gross coil impedance is needed. We think that success here hinges upon finding a tractable representation of the impedance "reflection factor" other than an asymptotic power series. Some preliminary considerations of a variational approach seem promising, and we shall pursue this route. Secondly, an adequate, tractable approximation to the previously mentioned Green's function must be found. This is not easy, even for idealized geometries. The difficulty is that one needs the Green's function near the metal-air interface and near the source (i.e., near the flaw) where it is difficult to represent the Green's function by any simple approximation; both its amplitude and phase change rapidly in the region of interest. A conventional expansion in orthogonal functions runs into difficulty because

many terms must be retained. A variational approach may succeed here also, and we shall pursue this as well as anything else that suggests itself.

On the experimental side we plan to interface our three-channel eddy current system with the newly installed College of Engineering PDP-11/70 real-time computing system (using funds from other sources) and to use it to test the validity of our theoretical work.

B. Microwave NDE

Work planned at 100 GHz has been delayed by long delivery times on essential components on order. (The 10 GHz work was undertaken primarily because of this). Vendors now promise delivery early in 1980 and, this obtaining, we shall immediately undertake already planned experiments on the scattering of 100 GHz waves by flaws in structural dielectrics. In addition to basic scattering studies, we shall attempt to image flaws by the synthesis of a large aperture using receiver scanning and coherent detection techniques.

APPENDIX A

IMPEDANCE OF A LOOP WITH A CYLINDRICAL CONDUCTING CORE*

S.A. Long, C.G. Gardner, A. Zaman, and S. Toomsawasdi
Electrical Engineering Department
University of Houston
Houston, Texas

Abstract

The change in complex impedance between an ideal one-turn coil surrounding and coaxial with an infinitely long circular cylinder of conductivity σ and permeability μ and a similar coil without the core has been calculated. From the exact expression a power series in (δ/b)(δ = skin depth; b = radius of core) has been developed. From this result the change in impedance of a physically realistic multi-turn coil can be estimated with reasonable accuracy. The theory permits a rational approach to optimization of the design of eddy current test coils and provides a basis for the later calculation of the effects of discontinuities in the core.

* This work was supported in part by the U. S. Air Force Office of Scientific Research through Grant #77-3457.

1. INTRODUCTION

A notable omission to the present body of knowledge dealing with eddy current testing is the lack of an adequate theoretical basis for the interpretation of changes in the impedance of the test coil. This deficiency remains, even though the fundamental theory is well established, owing to the mathematical difficulties involved in solving the equations for practical test-coil and specimen configurations. A complete solution in analytical form seems to exist for only a few idealized cases which do not necessarily approximate practical problems of current interest.

The program selected for study in this investigation is that of an idealized one-turn coil (or loop) around and coaxial with a long, solid, electrically conducting cylinder. This arrangement is illustrated in Figure 1

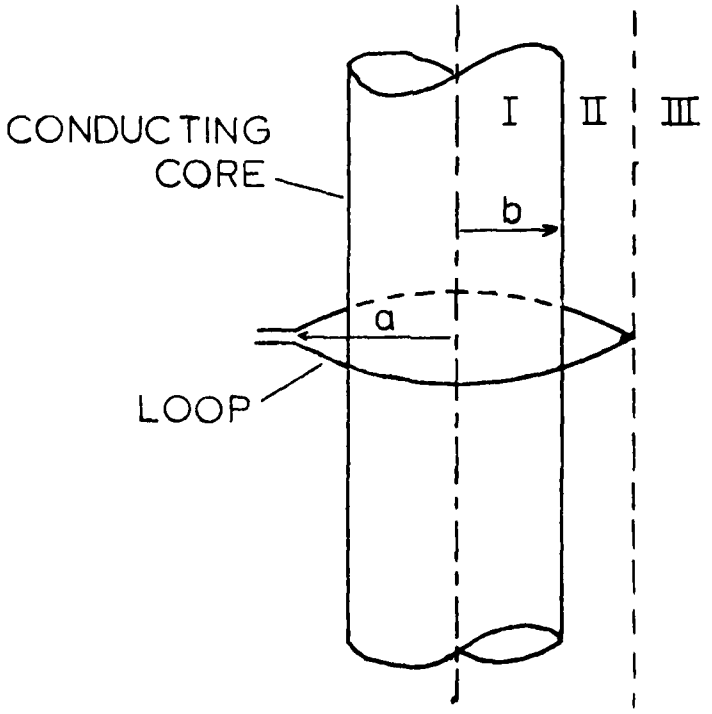

Figure 1 Loop with Cylindrical Core

and shows the loop with radius a and the core with radius b and conductivity σ. The theoretical treatment will assume that the core is infinitely long. (This approximation should produce very small errors as long as the distance from the position of the loop to either end of the core is large compared to the dimensions of the loop itself). This problem has the advantage of being simple enough to permit a meaningful approximate solution to be found while still corresponding to a practical eddy current testing situation. The results show how the complex impedance of the test coil changes when a cylindrical specimen is placed inside the loop and how this impedance is a function of the geometrical and material parameters of the cylindrical core.

2. THEORY

A theoretical treatment of a geometrically similar problem has been previously reported by Islam.[1] In this work, however, the emphasis was on the radiation properties of the configuration and thus only a high frequency approximation was attempted for the case of a magnetically permeable cylindrical core. The case of interest in this work, that of an electrically conducting core at much lower frequencies, may be attacked in a similar fashion but is essentially a completely different problem. From Maxwell's equations for time-harmonic fields one may derive the wave equation for the magnetic vector potential $\vec{A}$ in terms of the impressed current density $\vec{J}$.

$$\nabla^2\vec{A} + k^2\vec{A} = -\mu\vec{J}$$

Using the standard eddy current approximation of neglecting the displacement current terms and recognizing that the vector potential has only a $\hat{\phi}$ component which depends on r and z, the left hand side of the equation becomes

$$\nabla^2\vec{A} = \hat{\phi}(\nabla^2 A_\phi - \frac{A_\phi}{r^2}) = \hat{\phi}[\frac{1}{r}\frac{\partial}{\partial r}(r\frac{\partial A_\phi}{\partial r}) + \frac{\partial^2 A_\phi}{\partial z^2} - \frac{A_\phi}{r^2}]$$

$$= \hat{\phi}[\frac{\partial^2 A_\phi}{\partial r^2} + \frac{1}{r}\frac{\partial A_\phi}{\partial r} - \frac{A_\phi}{r^2} + \frac{\partial^2 A_\phi}{\partial z^2}]$$

Equating this expression to the source terms due to the loop current and the induced eddy currents one obtains the equation for the vector potential in each of the regions shown in Figure 1.

$$\frac{\partial^2 A_\phi}{\partial r^2} + \frac{1}{r}\frac{\partial A_\phi}{\partial r} - \frac{A_\phi}{r^2} + \frac{\partial^2 A_\phi}{\partial z^2} = \begin{cases} -\mu_0 i_0 \delta(z)\delta(a-r); & r>b \\ j\omega\mu\sigma A_\phi ; & r<b \end{cases}$$

where μ_0 is the permeability of free space, i_0 is the magnitude of the impressed loop current, ω is the angular frequency of the time-harmonic fields, and μ and σ are the permeability and conductivity of the core. The presence of the impressed loop current at z=0, r=a is represented by the two δ-functions.

The solution to the equation may be found using a cosine transform.

$$A_\phi(r,z) = \frac{1}{\pi}\int_0^\infty g(r,k)\cos kz\, dk$$

with the following functions defined for each of the three regions.

$$g(r,k) = \begin{cases} C_1 I_1[\sqrt{(k^2+j\kappa^2)}r] & r<b \\ C_2 I_1(kr)+C_3 K_1(kr) & b<r<a \\ C_4 K_1(kr) & r>a \end{cases}$$

where I_1 and K_1 are the modified Bessel functions of order one, $\kappa^2 = \omega\mu\sigma$, and C_1, C_2, C_3, and C_4 are constants to be determined by the boundary conditions.

Since the quantity of primary interest is the vector potential in the vicinity of the loop, the simplest expression is that for Region III for which only C_4 needs to be found from the standard boundary conditions.

$$C_4 = \mu_0 i_0 a \left\{ I_1(ka) + \left[\frac{kb\ I_0(kb)I_1(\gamma) - rI_0(\gamma)I_1(kb)}{ka\ I_1(\gamma)K_0(kb) + \gamma I_0(\gamma)K_1(ka)} \right] K_1(ka) \right\}$$

where I_0 and K_0 are the modified Bessel functions of order zero and $\gamma = \sqrt{(kb)^2 + j(\kappa b)^2}$. Using this expression the value of A_ϕ along the loop at z=0, r=a can be found.

$$A_\phi(a,0) = \frac{\mu_0 i_0 a}{\pi} \int_0^\infty I_1(ka)K_1(kr)dk + \frac{\mu_0 i_0 a}{\pi} \int_0^\infty \left[\frac{kb\ I_0(kb)I_1(\gamma) - \gamma I_0(\gamma)I_1(kb)}{kb\ I_1(\gamma)K_0(kb) + \gamma I_0(\gamma)K_1(kb)} \right] K_1^2(ka)dk$$

The first of these integrals can be shown to be exactly the contribution to the vector potential due to the loop itself if the core were not present at all. (This term is singular in nature.) The second integral is the contribution due to the eddy currents and thus represents the difference in the vector potential with and without the core present. This term now called ΔA_ϕ may be expanded as an asymptotic series.

$$\Delta A_\phi = \frac{\mu_0 i_0 a}{\pi} \left[-\int_0^\infty \frac{I_1(kb)K_1^2(ka)}{K_1(kb)} dk + \int_0^\infty \frac{T(\gamma)K_1^2(ka)}{K_1^2(kb)} dk - \int_0^\infty \frac{T^2(\gamma)kbK_0(kb)K_1^2(ka)}{K_1^3(kb)} dk + \ldots \right]$$

where $T(\gamma) = \frac{1}{\gamma} \frac{I_1(\gamma)}{I_0(\gamma)}$.

It should be noted that the dependence of ΔA_ϕ on the material parameters μ and σ of the core is completely contained in the $T(\gamma)$ term. Using the asymptotic series for the modified Bessel functions the following expressions can be found.

$$T(\gamma) \doteq \frac{1}{\gamma} - \frac{1}{2\gamma^2} + \ldots$$

and $$\gamma \doteq \sqrt{j}\kappa b = (1+j)\frac{b}{\delta}$$

where the skin depth is given by $\delta = \sqrt{\frac{2}{\omega\mu\sigma}}$. One may then divide the contributions to A_ϕ into real and imaginary parts.

$$\Delta A_\phi \doteq \frac{\mu_0 I_0 a}{\pi b} \{-N_0(\tfrac{a}{b}) + \tfrac{1}{2}(\tfrac{\delta}{b})N_1(\tfrac{a}{b}) - \tfrac{1}{4}(\tfrac{\delta}{b})^3[N_2(\tfrac{a}{b}) + N_3(\tfrac{a}{b})]\}$$

$$- j\frac{\mu_0 i_0 a}{\pi b} \{\tfrac{1}{2}(\tfrac{\delta}{b})N_1(\tfrac{a}{b}) - \tfrac{1}{2}(\tfrac{\delta}{b})^2[\tfrac{1}{2}N_1(\tfrac{a}{b}) + N_2(\tfrac{a}{b})]$$

$$+ \tfrac{1}{4}(\tfrac{\delta}{b})^3[N_2(\tfrac{a}{b}) + N_3(\tfrac{a}{b})]\}$$

where the following integrals have been defined and are seen to be only a function of the ratio a/b. ($\eta = kb$)

$$N_0(\tfrac{a}{b}) = \int_0^\infty \frac{I_1(\eta)K_1^2(\eta\frac{a}{b})}{K_1(\eta)}\,d\eta$$

$$N_1(\tfrac{a}{b}) = \int_0^\infty \frac{K_1^2(\eta\frac{a}{b})}{K_1^2(\eta)}\,d\eta$$

$$N_2(\tfrac{a}{b}) = \int_0^\infty \frac{\eta K_0(\eta)K_1^2(\eta\frac{a}{b})}{K_1^3(\eta)}\,d\eta$$

$$N_3(\tfrac{a}{b}) = \int_0^{\pi} \frac{\eta^2 K_0(\eta) K_1^2(\eta\,\tfrac{a}{b})}{K_1^4(\eta)}\, d\eta$$

The apparent change in the driving point impedance of the loop is

$$\Delta Z = \Delta R + j\omega\Delta L = \frac{j\omega\,\Delta A_\phi\, 2\pi a}{i_0}$$

From the previous expressions the changes in inductance and resistance can be found to third order in δ/b.

$$\Delta L = -2\mu_0 \frac{a^2}{b} \{N_0(\tfrac{a}{b}) - \tfrac{1}{2}(\tfrac{\delta}{b})N_1(\tfrac{a}{b}) + \tfrac{1}{4}(\tfrac{\delta}{b})^3[N_2(\tfrac{a}{b}) + N_3(\tfrac{a}{b})]\}$$

$$\Delta R = 2\omega\mu_0 \frac{a^2}{b} \{\tfrac{1}{2}(\tfrac{\delta}{b})N_1(\tfrac{a}{b}) - \tfrac{1}{2}(\tfrac{\delta}{b})^2[\tfrac{1}{2}\,N_1(\tfrac{a}{b}) + N_2(\tfrac{a}{b}) + \tfrac{1}{4}(\tfrac{\delta}{b})^3[N_2(\tfrac{a}{b}) + N_3(\tfrac{a}{b}]\}$$

To obtain numerical values for ΔL and ΔR it is first necessary to evaluate the integrals N_0, N_1, N_2 and N_3. Although they cannot be evaluated analytically they can be found numerically for fixed values of the geometrical parameter a/b. Once these integrals are evaluated the expressions are each seen to be a power series in the parameter δ/b which contains the electrical properties of the core material. One should note that for the case of a perfectly conducting core (i.e. $\delta/b = 0$)

$$\Delta L = \frac{-2\mu_0 a^2}{b} N_0(\tfrac{a}{b})$$

and $\Delta R = 0$.

This is a reasonable result which shows a decrease in the inductance but no change in the resistance since no losses are possible. The effect of a large but finite conductivity is seen to diminish the amount of decrease found for the perfectly conducting case and to add a finite, positive apparent resistance.

3. RESULTS

To facilitate the evaluation of ΔL and ΔR for practical cases the integrals N_0, N_1, N_2, and N_3 were evaluated for several values of a/b varying from a value of 1.05 to 2.0. Using these results the values of ΔR and ΔL can be calculated through terms of order $(\delta/b)^3$. Accuracy of the results depends critically on the assumption that δ/b remains small with respect to one.

For the case of an aluminum core with a 3/4" diameter we find $\delta = .0826/\sqrt{f}$ which for f = 50 KHz yields a skin depth δ = 0.37 mm resulting in a value of $\delta/b = .0388$. Thus for this practical case we are well within the assumptions used in the derivations.

To generalize the results somewhat the normalized quantities $\Delta R/\omega\mu a$ and $\Delta X/\omega\mu a$ have been plotted in the remaining figures ($\Delta X = \omega\Delta L$). It should be noted that each of these quantities are unitless. The most obvious graphical presentations would be those of ΔR and ΔL versus the geometrical parameter a/b and the material parameter δ/b. Unfortunately this direct approach does not correspond to the usual parameters which may be subject to change. Assuming that the practical testing situation consists of a cylindrical sample moving through a fixed coil the quantities which may change are actually the radius of the core b and the conductivity of the core material σ. To illustrate the changes in impedance for variations in

b about a nominal radius b_0, the graphs in Figures 2 and 3 are shown. In Figure 2 the normalized change in resistance is shown versus the quantity b/b_0. The nominal radius b_0 may be any value as long as our restriction of $\delta/b_0 << 1$ is satisfied. The value of $a/b_0 = 1.25$ was chosen to be representative of a real coil design which couples strongly with the core. A family of curves is also shown for several values of δ/b_0. It is noted that all the curves approach zero as b/b_0 is decreased and become very large as b/b_0 approaches 1.25 which is the position of the driving loop. A similar set of curves is shown in Figure 3 for the change in reactance. Again as expected the change in reactance approaches zero as the core radius decreases and becomes a very large negative value for b/b_0 near 1.25. It should be noted that changes in the parameter δ/b_0 have a relatively small effect on ΔX as compared to their effect on ΔR. The same functional dependence is also illustrated in Figure 4. The solid curves show the normalized resistance plotted versus the normalized reactance as b/b_0 is varied. Changes in the complex impedance can be seen for varying radii for each of four values of δ/b_0.

The effect of changes in conductivity of the core on the resistance and the reactance are shown in Figures 5 and 6. The conductivity is again normalized with respect a σ_0 near that of aluminum. (However, σ_0 is actually arbitrary as long as the condition that $\delta/b << 1$ is still satisfied). The limiting behavior is again logical showing the resistance approaching zero for large conductivities and zero for very small values. The reactance is seen to approach the "perfect conductor" case as σ increases. The region where σ becomes small violates the assumption on δ/b and therefore the behavior of these curves ther has no meaning. The resistance versus the

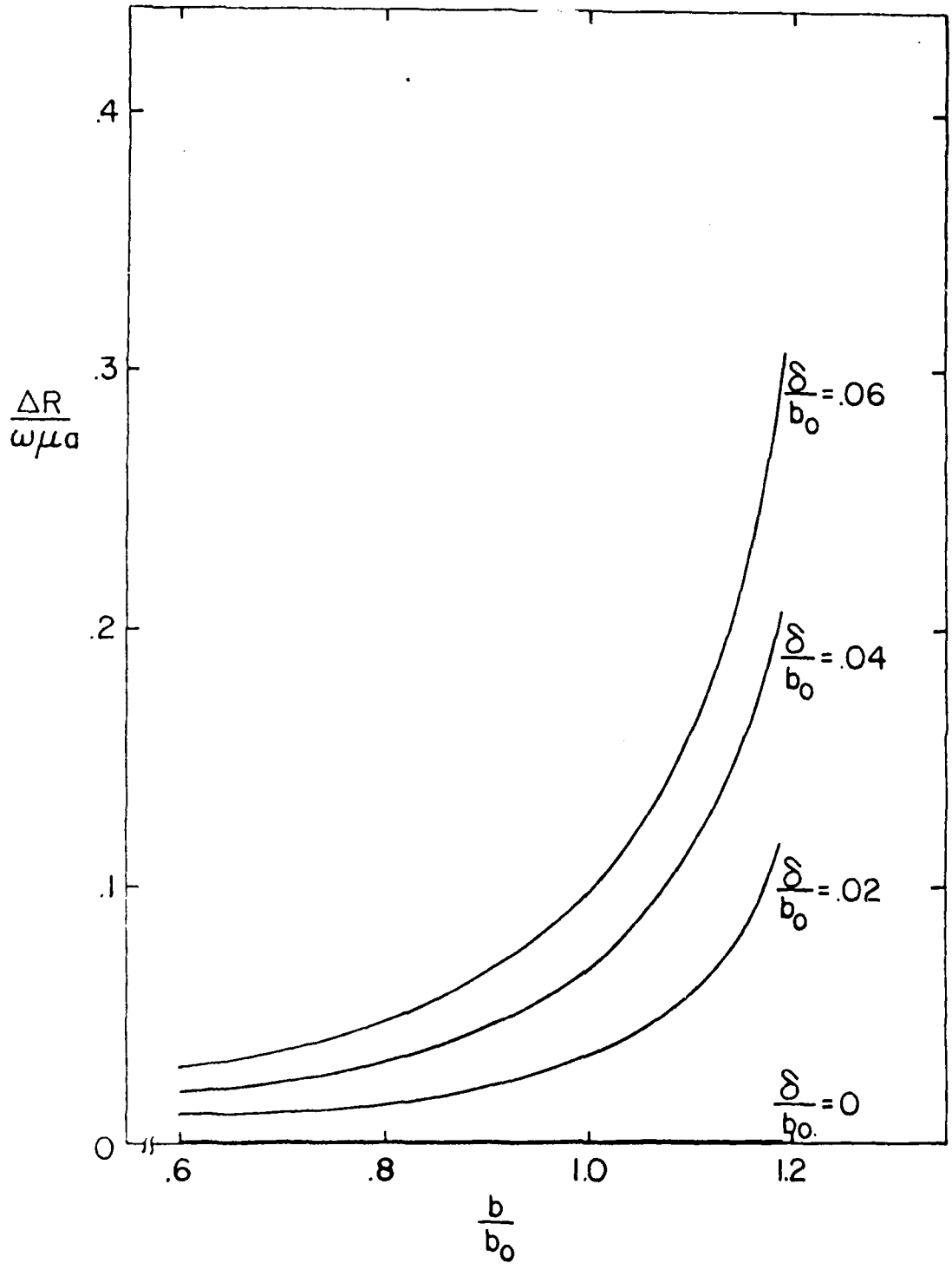

Figure 2 Normalized Resistance Versus Core Radius

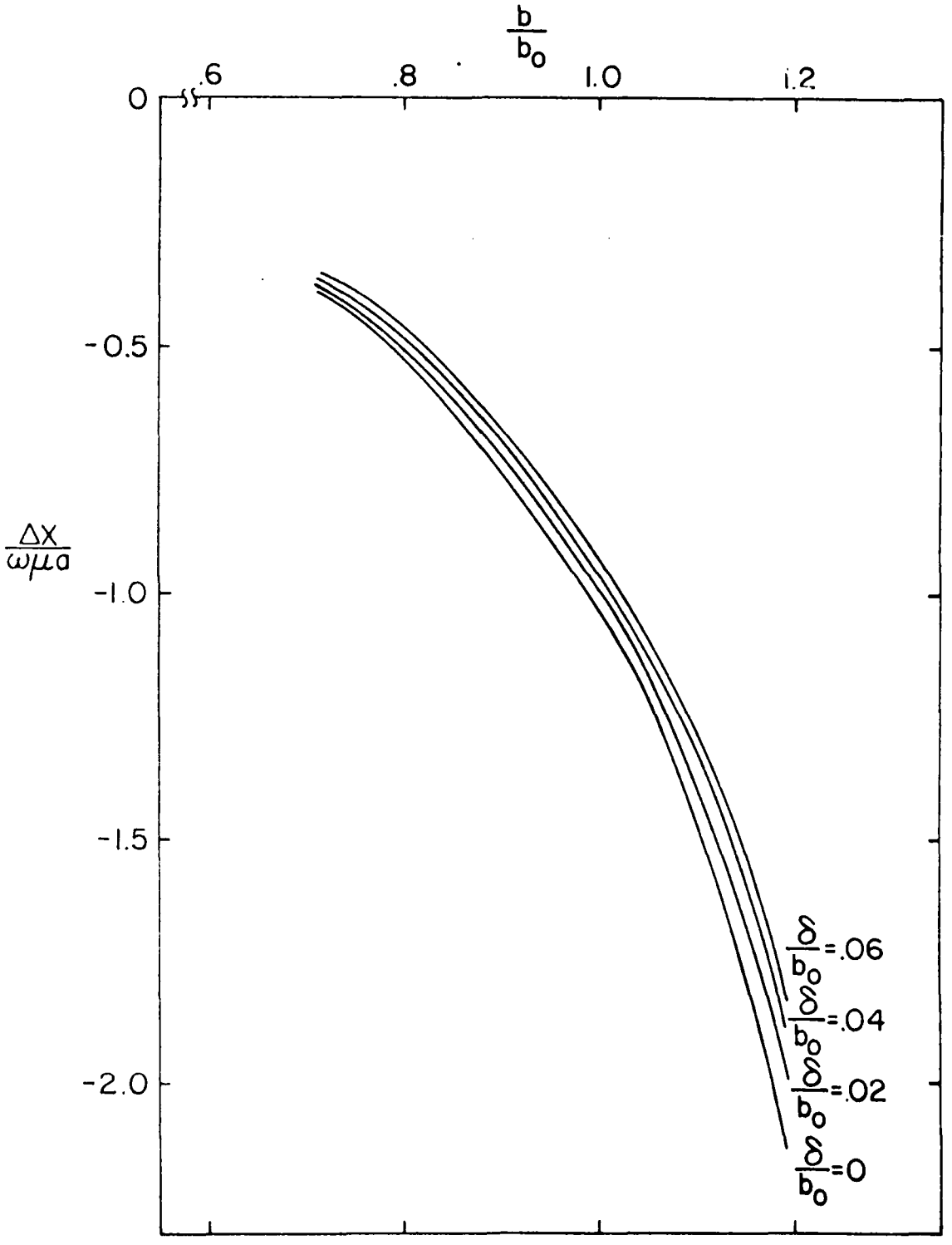

Figure 3 Normalized Reactance Versus Core Radius

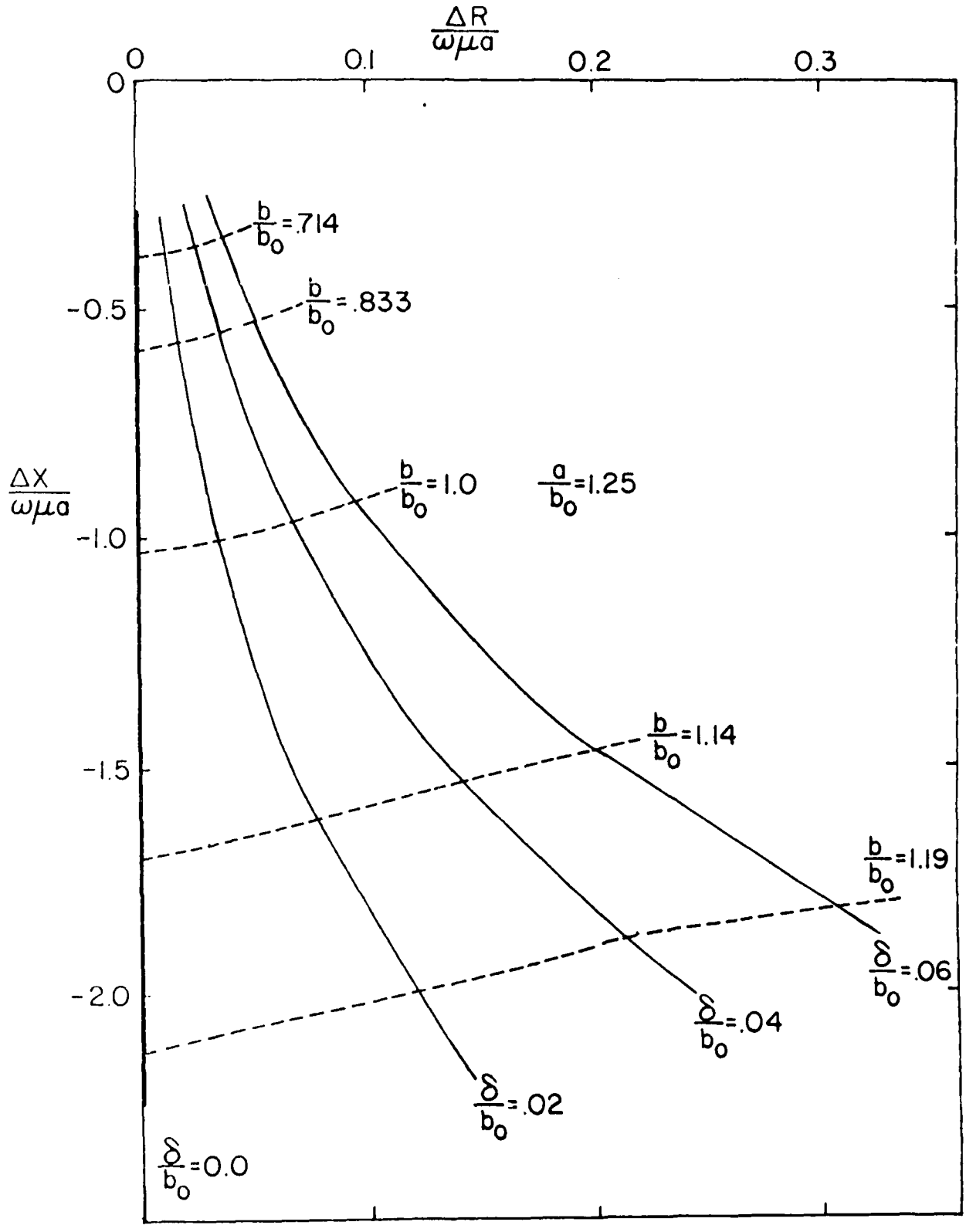

Figure 4 Resistance Versus Reactance as Core Radius Changes

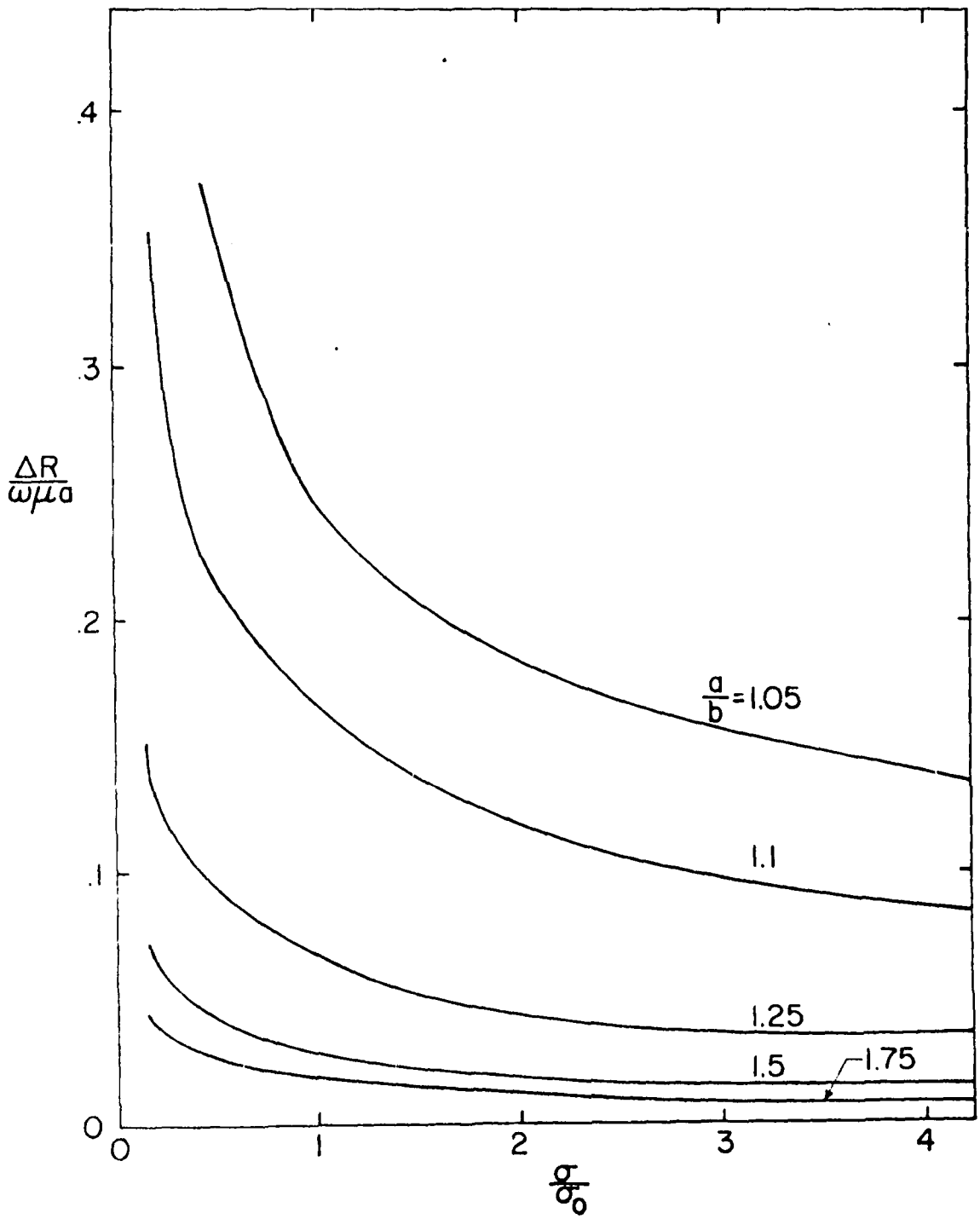

Figure 5 Normalized Resistance Versus Conductivity

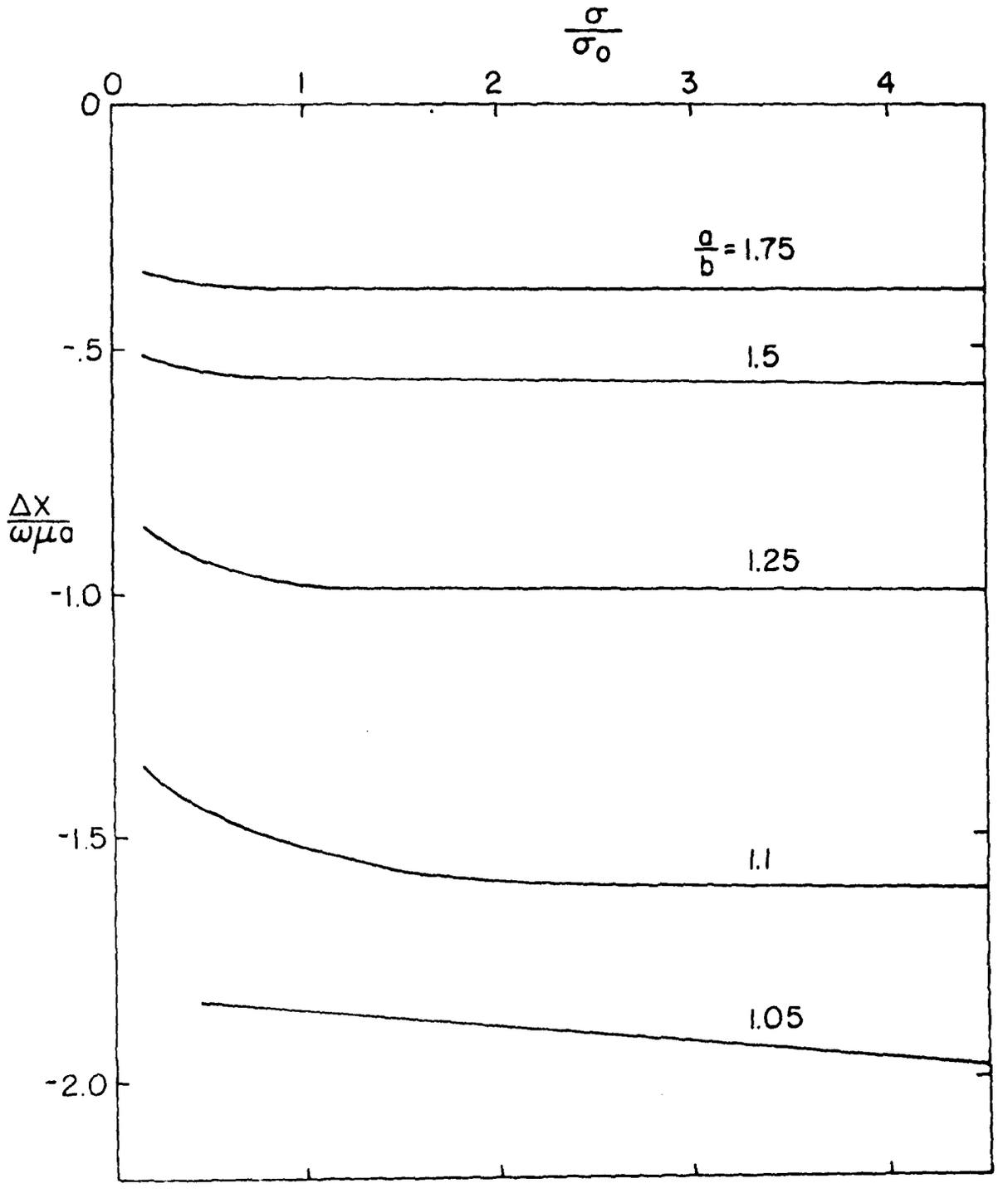

Figure 6 Normalized Reactance Versus Conductivity

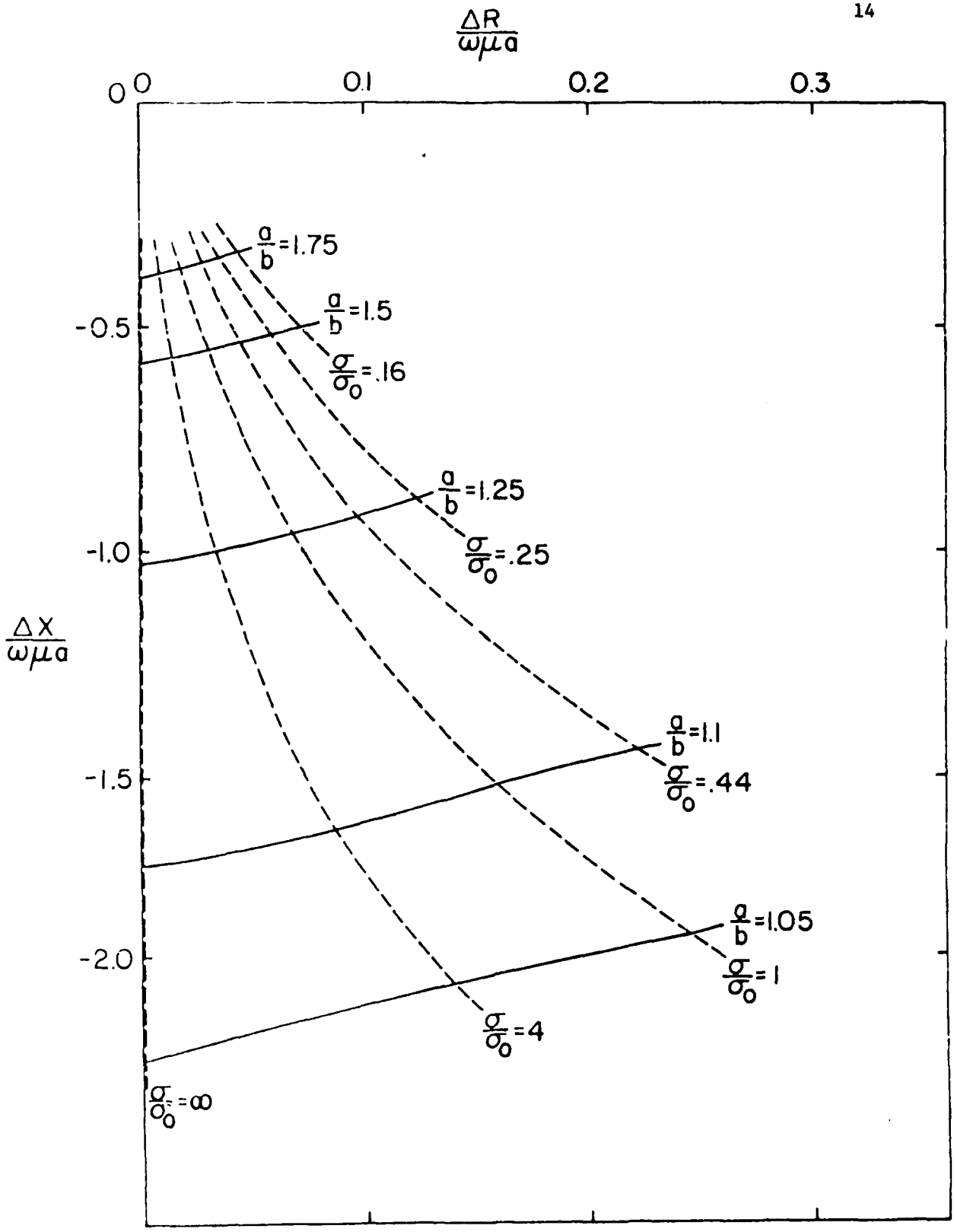

Figure 7 Resistance Versus Reactance as Conducting Changes

reactance is shown in the solid lines of Figure 7. As the conductivity decreases from the perfect conductor case ΔR is seen to increase while ΔX becomes less negative. Each of these curves terminates in the region where the assumption that $\delta/b << 1$ begins to break down.

With the aid of Figures 4 and 7 one may ascertain the behavior of changes in both the resistance and reactance for any percent change in either the radius of the core or its conductivity. The functional change in impedance is quite different for the two parameters. This characteristic may therefore be utilized in practical testing to determine changes in sample radius and conductivity.

4. REFERENCE

(1) Islam, A. M., "A Theoretical Treatment of Low-Frequency Loop Antennas with Permeable Cores", IEEE Trans. on Antennas and Propagation, Vol. AP-11, No. 2, March 1963, pp. 162-169.

APPENDIX B

The Impedance of a Single-Turn Coil Near A Conducting Half-Space

Afroz J. M. Zaman, Stuart A. Long and C. Gerald Gardner
Department of Electrical Engineering
University of Houston
Houston, Texas 77004

Abstract

The change in complex impedance between an ideal one-turn circular coil located above and parallel to a conducting half-space with respect to a similar isolated coil has been calculated. From this result a series expansion of the integrand allows the solution to be approximated by terms expressed as complete elliptic integrals. Results have been calculated for the change in impedance as a function of the lift-off distance and the conductivity of the half-space for a coil of representative radius.

This work was supported in part by the U. S. Air Force Office of Scientific Research through Grant No. 77-3457.

1. INTRODUCTION

The eddy current method of nondestructive evaluation entails the induction of eddy currents in a conductive test object by a time-varying field produced by a suitable distribution of impressed currents (via an excitation or primary coil), and the detection of the resultant field, usually by an inductive search coil which may be either a separate secondary coil or the primary coil itself. (See Figure 1.) The method is ordinarily used at frequencies sufficiently low to neglect effects due to displacement current; hence a theoretical analysis entails calculating either a transfer impedance for a primary coil and secondary coil in the presence of the test object, or the calculation of the self impedance of a primary coil in the presence of the test object. In practice one often needs only the change in impedance produced by the test object or by changes in the nominal properties of the test object (e.g. changes in its geometry or position with respect to the test coil or coils, or distributed or localized changes in the resistivity of the test object). The most general case, allowing arbitrary configurations of primary and secondary coils and arbitrary test objects can be handled only by numerical methods. Certain idealized arrangements can be treated analytically either exactly or in useful approximation. In virtually all cases of practical interest, the analysis eventually reduces to the evaluation of certain integrals which cannot be expressed in closed form in terms of standard transcendental functions.

In this paper we discuss the case of a one-turn circular coil located above and parallel to the surface of a homogeneous conductive half-space. From the standard boundary value problem approach we obtain the general

expression for the change in coil impedance, ΔZ, produced by the half-space; ΔZ is given in terms of an integral over a separation parameter. A series expansion of one term in the integrand permits the integral to be expressed as a series of terms each of which is expressible in terms of complete elliptic integrals. The leading terms of this series approximate ΔZ asymptomatically for sufficiently small values of skin depth of the half-space.

The problem addressed here has previously been treated by Cheng [1] who evaluated ΔZ by numerical methods for various choices of the relevant parameters. Similarly, Dodd and Deeds [2] have devised a digital computer program capable of handling circular test coils in the presence of layered planar and coaxial cylindrical test objects. Such brute force numerical procedures are valuable for design purposes, but have the disadvantage of somewhat concealing the essentially simple manner in which the final result depends upon the parameters of the problem. The approach taken here, while less universal than the purely numerical approach; results in relatively simple, though approximate and restricted, formulas for ΔZ in terms of the basic parameters of the problem.

For illustrative and comparative purposes, some selected numerical examples are also given.

II. Theoretical Analysis

The basic geometry of the problem is shown in Figure 1 and consists of a loop of radius r_0 oriented parallel to and at a distance ℓ above a homogeneous half-space of conductivity σ. Beginning with the basic equation for the vector potential

$$\nabla^2\vec{A} + k^2\vec{A} = -\mu_0 I(t)\,\frac{\delta(r_0-r)}{r}\,\delta(\ell-z) \qquad (1)$$

and noting the symmetry of the problem, it is seen that the only component of the vector potential present is the circumferential component, A_ϕ, and that A_ϕ is a function of r and z only. Making the usual low-frequency, quasi-static approximation that the $k^2\vec{A}$ term is negligible for z>0, we have:

$$\nabla^2\vec{A} = \frac{\partial^2 A_\phi}{\partial r^2} + \frac{1}{r}\frac{\partial A_\phi}{\partial r} + \frac{\partial^2 A_\phi}{\partial z^2} - \frac{A_\phi}{r^2} = 0 \quad \text{for } z>0 \qquad (2)$$

and, with $k^2 \doteq -j\omega\mu\sigma$ for z<0 :

$$\frac{\partial^2 A_\phi}{\partial r^2} + \frac{1}{r}\frac{\partial A_\phi}{\partial r} + \frac{\partial^2 A_\phi}{\partial z^2} - \frac{A_\phi}{r^2} - j\omega\mu\sigma A_\phi = 0 \text{ for } z<0 \qquad (3)$$

Solving by the separation of variables technique yields the following expression for the general solution to Equations (2) and (3).

$$A_\phi(r,z) = \int_0^\infty [A(\alpha)e^{\alpha z}+B(\alpha)e^{-\alpha z}][C(\alpha)J_1(\alpha r)+D(\alpha)Y_1(\alpha r)]d\alpha \qquad (4)$$

where α is the separation constant. Since z may become infinitely large in the region $z>\ell$, the coefficient $A(\alpha)$ must equal zero. Similarly in the region $z<0$ $B(\alpha)$ must also equal zero, and since the origin is included in all regions, then $D(\alpha)$ must equal zero in each.

$$A_{\phi 1}(r,z) = \int_0^\infty B_1 e^{-\alpha z} J_1(\alpha r)d\alpha \qquad z>\ell>0 \qquad (5)$$

$$A_{\phi 2}(r,z) = \int_0^\infty [C_2 e^{\alpha z}+B_2 e^{-\alpha z}]J_1(\alpha r)d\alpha \qquad \ell>z>0 \qquad (6)$$

$$A_{\phi 3}(r,z) = \int_0^\infty C_3 e^{\alpha_1 z} J_1(\alpha r)\,d\alpha \qquad z<0 \qquad (7)$$

where $\alpha_1^2 = \alpha^2 + j\omega\mu\sigma$.

Since the electric field is proportional to A_ϕ, the boundary conditions for the tangential electric field can be satisfied by equating the values of A_ϕ at the $z = \ell$ plane.

$$\int_0^\infty B_1 e^{-\alpha\ell} J_1(\alpha r)\,d\alpha = \int_0^\infty (C_2 e^{\alpha\ell} + B_2 e^{-\alpha\ell}) J_1(\alpha r)\,d\alpha \qquad (8)$$

Multiplying both sides by the integral operator $\int_0^\infty \{\ldots\} J_1(\alpha' r) r\,dr$ and using the Fourier-Bessel identity [3]

$$\int_0^\infty J_1(\alpha r) J_1(\alpha' r) r\,dr = \frac{\delta(\alpha-\alpha')}{\alpha} \qquad (9)$$

gives the following result:

$$\frac{B_1 e^{-\alpha'\ell}}{\alpha'} = \frac{C_2}{\alpha'} e^{\alpha'\ell} + \frac{B_2}{\alpha'} e^{-\alpha'\ell} \qquad (10)$$

or

$$B_1 e^{-\alpha\ell} = C_2 e^{\alpha\ell} + B_2 e^{-\alpha\ell} \qquad (11)$$

The radial component of the magnetic field can also be found from the vector potential; $H_r = -\frac{\partial}{\partial z} A_\phi$. H_r is discontinuous at the position of the loop ($r=r_0$, $z=\ell$) by an amount equal to the surface current density there.

$$\left[-\frac{\partial}{\partial z} A_{\phi 1} + \frac{\partial}{\partial z} A_{\phi 2}\right]_{z=\ell} = \mu I\, \delta(r-r_0) \qquad (12)$$

or

$$-B_1 e^{-\alpha \ell} = C_2 e^{\alpha \ell} - B_2 e^{-\alpha \ell} - \mu I r_0 J_1(\alpha r_0) \tag{13}$$

Similarly the boundary conditions may also be applied at z = 0 where bo
E_ϕ and H_r are continuous, yielding

$$C_2 + B_2 = C_3 \tag{14}$$

and

$$C_2 - B_2 = \frac{\alpha_1}{\alpha} C_3 \tag{15}$$

These four Equations (11, 13, 14 and 15) can then be solved for the con
B_1, C_2, B_2, and C_3 and used in Equations (5), (6), and (7) to e uate
vector potential.

Since our principle interest lies in evaluating the vector potenti
at the location of the loop the most direct route is to evaluate the co
stant B_1:

$$B_1 = \frac{\mu I r_0 J_1(\alpha r_0)}{2} \left[e^{\alpha \ell} + e^{-\alpha \ell} \frac{(1 - \frac{\alpha_1}{\alpha})}{(1 + \frac{\alpha_1}{\alpha})} \right] \tag{16}$$

Thus

$$A_{\phi 1}(r,z) = \frac{\mu I r_0}{2} \int_0^\infty J_1(\alpha r_0) J_1(\alpha r) e^{(-\alpha z - \alpha \ell)} \left[e^{+2\alpha \ell} + (\frac{\alpha - \alpha_1}{\alpha + \alpha_1}) \right] d\alpha \tag{17}$$

The two terms in the square brackets represent respectively the vector
potential due to the loop itself and that due to the currents induced i
the conducting plane. This second term due to the conductive half-spac

will produce the change in impedance from the case of the isolated loop to the case of the loop near the plane. This change in vector potential is thus given by this second term.

$$\Delta A_{\phi 1}(r,z) = \frac{\mu I r_0}{2} \int_0^\infty J_1(\alpha r_0) J_1(\alpha r) e^{-\alpha(z+\ell)} \left(\frac{\alpha-\alpha_1}{\alpha+\alpha_1}\right) d\alpha \qquad (18)$$

This change in vector potential can be used to calculate the change in impedance due to the presence of the conductor by integrating the tangential electric field around the position of the loop:

$$\Delta Z = \frac{-\oint \Delta\vec{E}\cdot d\vec{\ell}}{I} = j\omega \frac{2\pi r_0}{I} \Delta A_{\phi 1}(r_0,\ell) \qquad (19)$$

since $\Delta\vec{E} = -j\omega\Delta A_{\phi 1}\,\hat{\phi}$.

$$\Delta Z = \pi\omega r_0^2 j \int_0^\infty J_1^2(\alpha r_0) e^{-2\alpha\ell} \left(\frac{\alpha-\alpha_1}{\alpha+\alpha_1}\right) d\alpha \qquad (20)$$

The integrand factor $(\alpha-\alpha_1)/(\alpha+\alpha_1)$, essentially a reflection factor, has modulus equal to or less than unity, the extreme value being assumed for $\alpha=0$ and $\alpha=\infty$. The integrand factor $J_1^2(\alpha r_0)$ guarantees that the value of the integral is negligibly affected by values of α greater than about, $10/r_0$. Practical values of r_0 are usually of the order of 10^{-2}m. For such values of r_0 the important range for α is $0 \leq \alpha \leq 10^3 m^{-1}$, while the quantity $\omega\mu_0\sigma$ [$= 2/(\text{skin depth})^2$] is, in many practical cases, of the order of 10^7 (e.g., for aluminum at 50 KHz, $\omega\mu_0\sigma = 1.5\times10^7$). For such cases, $\alpha^2/\omega\mu_0\sigma \leq 0.1$, and $(\alpha-\alpha_1)(\alpha+\alpha_1)$ may be expanded as a power series in $\alpha/\sqrt{\omega\mu_0\sigma}$:

$$\frac{\alpha-\alpha_1}{\alpha+\alpha_1} = -1 + \frac{2}{\sqrt{j}}\frac{\alpha}{\kappa} - \frac{2}{j}\frac{\alpha^2}{\kappa^2} + \ldots = -1 + (1-j)(\alpha\delta) + j(\alpha\delta)^2 + \ldots$$

where $\delta = \sqrt{2/\omega\mu_0\sigma}$, and $\kappa = \sqrt{\omega\mu_0\sigma}$.

We expect the series above to converge rapdily provided $\alpha\delta<<1$. As we shall presently show, it is convenient to adopt r_0 as a characteristic length. Since the value of ΔZ is determined almost entirely by values of α for which $\alpha r_0 \leq 10$, we have rapid convergence of the integrated series if $\delta/r_0<<1/10$. Separating ΔZ into real and imaginary parts we have:

$$\Delta Z = \Delta R + j\Delta X \tag{22}$$

$$\Delta X = -\mu_0\omega\pi r_0^2\{\int_0^\infty J_1^2(\alpha r_0)e^{-2\alpha\ell}d\alpha - \int_0^\infty \delta J_1^2(\alpha r_0)e^{-2\alpha\ell}\alpha d\alpha\} \tag{23}$$

$$\Delta R = \mu_0\omega\pi r_0^2\{\int_0^\infty \delta J_1^2(\alpha r_0)e^{-2\alpha\ell}\alpha d\alpha - \int_0^\infty \delta^2 J_1^2(\alpha r_0)e^{-2\alpha\ell}\alpha^2 d\alpha\} \tag{24}$$

These changes in resistance and reactance can be represented by three integrals:

$$\Delta X = -\pi\omega\mu_0 r_0(I_1(\beta) - (\frac{\delta}{r_0})I_2(\beta)) \tag{25}$$

$$\Delta R = \pi\omega\mu_0 r_0((\frac{\delta}{r_0})I_2(\beta) - (\frac{\delta}{r_0})^2 I_3(\beta)) \tag{26}$$

where

$$\beta = 2\ell/r_0 \tag{27}$$

and

$$I_1(\beta) \doteq \int_0^\infty J_1^2(x) e^{-\beta x} dx \tag{28}$$

$$I_2(\beta) \doteq -\frac{d}{d\beta} I_1(\beta) \tag{29}$$

$$I_3(\beta) \doteq \frac{d^2}{d\beta^2} I_1(\beta) \tag{30}$$

$I_1(\beta)$ is just the Laplace transform of $J_1^2(x)$ [4]:

$$I_1(\beta) = \frac{1}{\pi} Q_{1/2}(1 + \frac{1}{2}\beta^2) \tag{31}$$

where $Q_{1/2}$ is the Legendre function of the second kind of order 1/2.

$I_2(\beta)$ is therefore given by

$$I_2(\beta) = -\frac{\beta}{\pi} Q'_{1/2}(1 + \frac{1}{2}\beta^2) \tag{32}$$

where the prime indicates differentiation with respect to the argument. The required derivative may be found from the recursion relation [5]

$$(x^2-1)Q'_{1/2}(x) = \frac{x}{2} Q_{1/2}(x) - \frac{1}{2} Q_{-1/2}(x) \tag{33}$$

For convenience in evaluation, both $Q_{1/2}$ and $Q_{-1/2}$ may be expressed in terms of complete elliptic integrals [5]:

$$Q_{1/2}(x) = x(\frac{2}{x+1})^{1/2} K[(\frac{2}{x+1})^{1/2}] - [2(x+1)]^{1/2} E[(\frac{2}{x+1})^{1/2}] \tag{34}$$

$$Q_{-1/2}(x) = (\frac{2}{x+1})^{1/2} K[(\frac{2}{x+1})^{1/2}] \tag{35}$$

where K(k) and E(k) are respectively the complete elliptical integrals of the first and second kind of modulus k:

$$K(k) = \int_0^{\pi/2} (1-k^2\sin^2 t)^{-1/2} dt \tag{36}$$

$$E(k) = \int_0^{\pi/2} (1-k^2\sin^2 t)^{1/2} dt \tag{37}$$

Values of K(k) and E(k) may be obtained from standard tables or from readily available computer software.

$I_3(\beta)$ may likewise be reduced to an expression involving K(k) and E(k). However, for most practical cases, the factor $(\delta/r_0)^2$ by which $I_3(\beta)$ is multiplied is so small that the contribution to ΔR from the term proportional to $I_3(\beta)$ is negligible.

III. Results

To illustrate the changes in impedance as a function of the lift-off distance ℓ and the conductivity σ, calculations were made for a loop of radius r_0 = 1.27 cm (diameter of one inch) at distances ℓ from .05 to 1.5 cm, and for conductivities from 0.1 to 4 times that of aluminum ($\sigma_0 = 3.8\times10^7$ mho/m). These results are shown in Figures 2 and 3 as a function of ℓ for various constant conductivities. The normalized dimensionless changes in impedance $\Delta X/\omega\mu r_0$ and $\Delta R/\omega\mu r_0$ are chosen as the quantities to be plotted. For all values of conductivity the value of $\Delta X/\omega\mu r_0$ is seen to approach a large negative value as ℓ decreases showing the known decrease in total inductance as the loop approaches the plane. As ℓ becomes large $\Delta X/\omega\mu r_0$ approaches zero as required. Similarly in Figure 2 $\Delta R/\omega\mu r_0$ is seen to give a large positive contribution for small ℓ and approaches zero as ℓ becomes

large.

To illustrate the effects of the conductivity on the changes in impedance for several constant values of lift-off, the results for the same loop are shown in Figures 4 and 5. The change in reactance $\Delta X/\omega\mu r_0$ is seen to be very nearly independent of conductivity over the range considered. The value of $\Delta R/\omega\mu r_0$, however, is seen to increase for lower values of σ. This resistance term, of course, approaches zero as the conductivity approaches that of a perfect conductor.

Both the variations in resistance and reactance can be combined into the one graph shown in Figure 6 by plotting ΔX versus ΔR. The solid lines thus show the change in impedance as the lift-off is changed, while the dashed lines show the variation with changing conductivity for constant lift-off ℓ.

The limiting values of $\Delta X/\omega\mu r_0$ for large values of σ can be checked by comparing the calculated values with that of the case of a loop above a perfectly conducting plane. Using image theory the mutual inductance between two identical loops located a distance 2ℓ apart can be calculated [6]:

$$M = 2.54\ N r_0$$

where N is a tabulated function of r_0 and ℓ. The values of M and ΔL at 50 KHz are compared in Table 1 and quite good agreement is found.

IV. Conclusions

For the commonly occurring case where $\delta << 0.1\ r_0$, the change in coil inductance is essentially the value that would occur if the substrate were

perfectly conductive; ΔL is thus dominated by its dependence on lift-off. The change in resistance is, for constant lift-off, proportional in first order to skin depth (or, for constant frequency, proportional to the square root of substrate conductivity); however, ΔR is also strongly dependent upon lift-off. Second-order changes in ΔL and ΔR, due to small variations in ℓ and σ about nominal values, are well approximated by linear functions of $\Delta\ell$ and $\Delta\sigma$, hence variations in ΔL and ΔR may readily be interpreted in terms of corresponding variations in lift-off conductivity.

REFERENCES

[1] David H. S. Cheng, The Reflected Impedance of a Circular Coil in the Proximity of a Semi-Infinite Medium, IEEE Transactions on Instrumentation and Measurement. V. 14, No. 3, pp. 107-116, September 1965.

[2] C. V. Dodd and W. E. Deeds, AnalyticalSolutions to Eddy-Current Probe-Coil Problems, J. Applied Physics, V. 39, No. 6, pp. 2829-2838, 1968.

[3] G. Arfken, Mathematical Methods for Physicists, 2nd ed., p. 495, Academic Press, N. Y., 1970.

[4] A. Erdelyi et. al., Tables of Integral Transforms, V. 1, p. 183, McGraw-Hill, Inc., 1954.

[5] M. Abramowitz and I. Stegun, Handbook of Mathematical Functions, pp. 334-337, 9th ed., Dover Publications, Inc., N. Y., 1970.

[6] F. E. Terman, Radio Engineers Handbook, p. 67, McGraw-Hill Book Co., Inc., N. Y., 1943.

List of Captions

Figure 1 Geometrical configuration of loop near a conductor.

Figure 2 Change in normalized resistance versus lift-off distance.

Figure 3 Change in normalized reactance versus lift-off distance.

Figure 4 Change in normalized resistance versus conductivity.

Figure 5 Change in normalized reactance versus conductivity.

Figure 6 Change in reactance versus change in resistance.

Table 1 Comparison of theoretical change in inductance to mutual inductance for perfect conductor case.

TABLE 1

ℓ (cm)	$\frac{\Delta X}{\omega \mu r_0}$	ΔL (μH)	M (μh)
2.5	1.0887	.01737	.01727
5.0	.5425	.00866	.00869
15.0	.07784	.00124	.00114

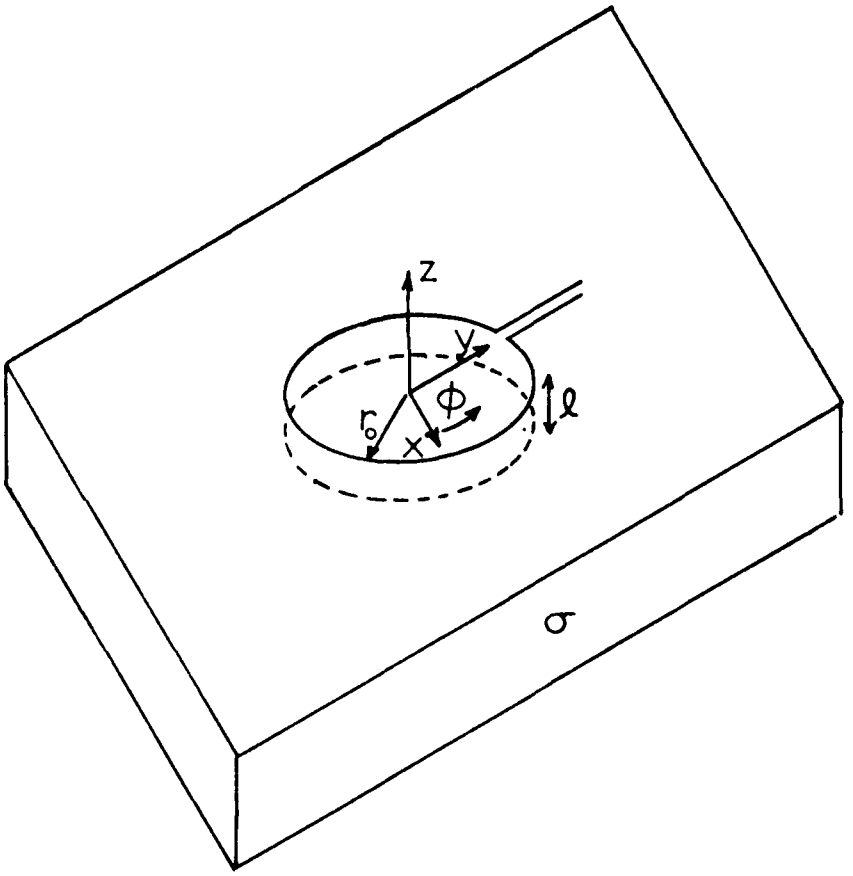
z
y
r_o
x
ϕ
ℓ
σ

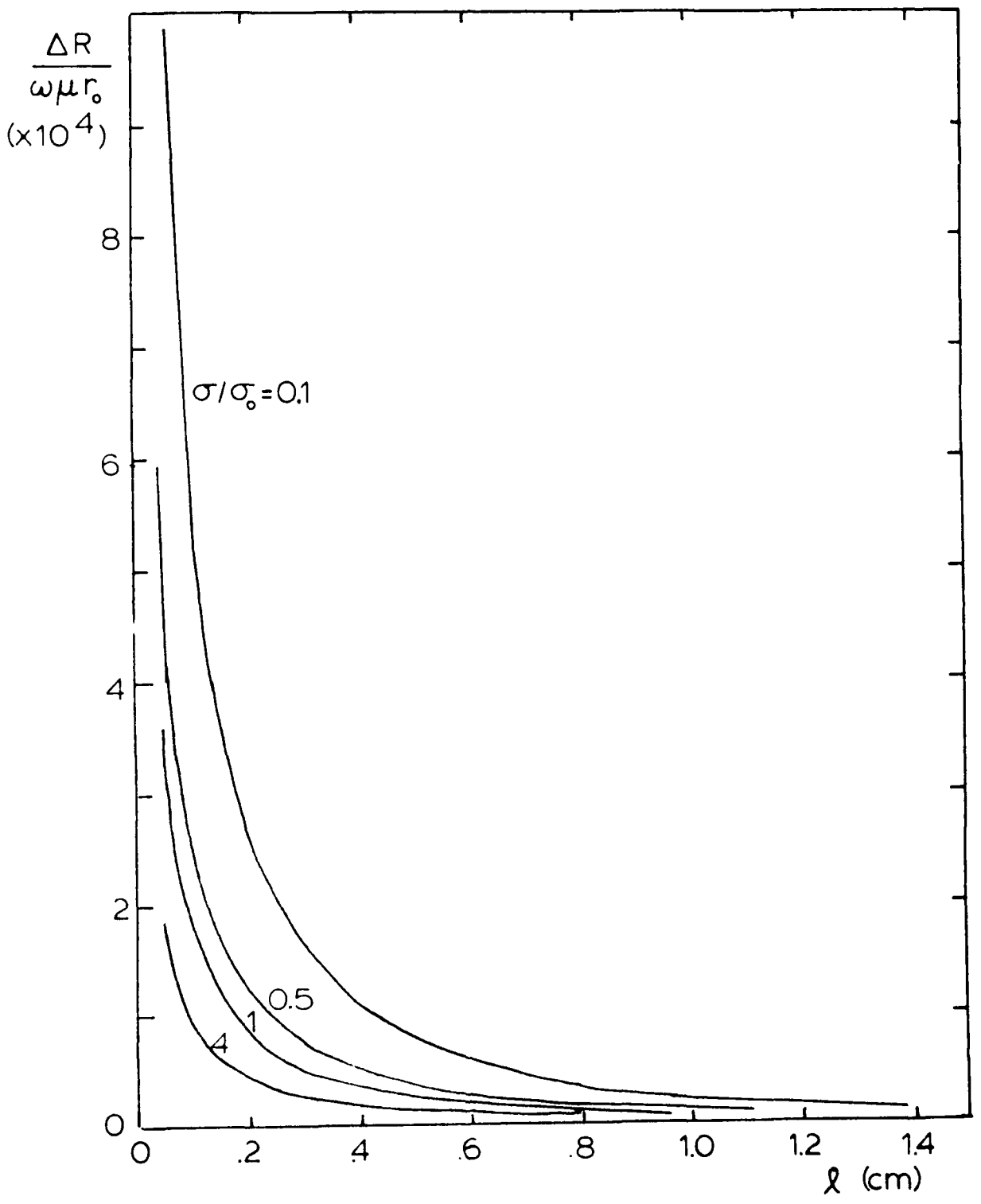
ΔR / ωμr₀ (×10⁴)
8
6
4
2
0
σ/σ₀=0.1
0.5
1
4
0
.2
.4
.6
.8
1.0
1.2
1.4
ℓ (cm)

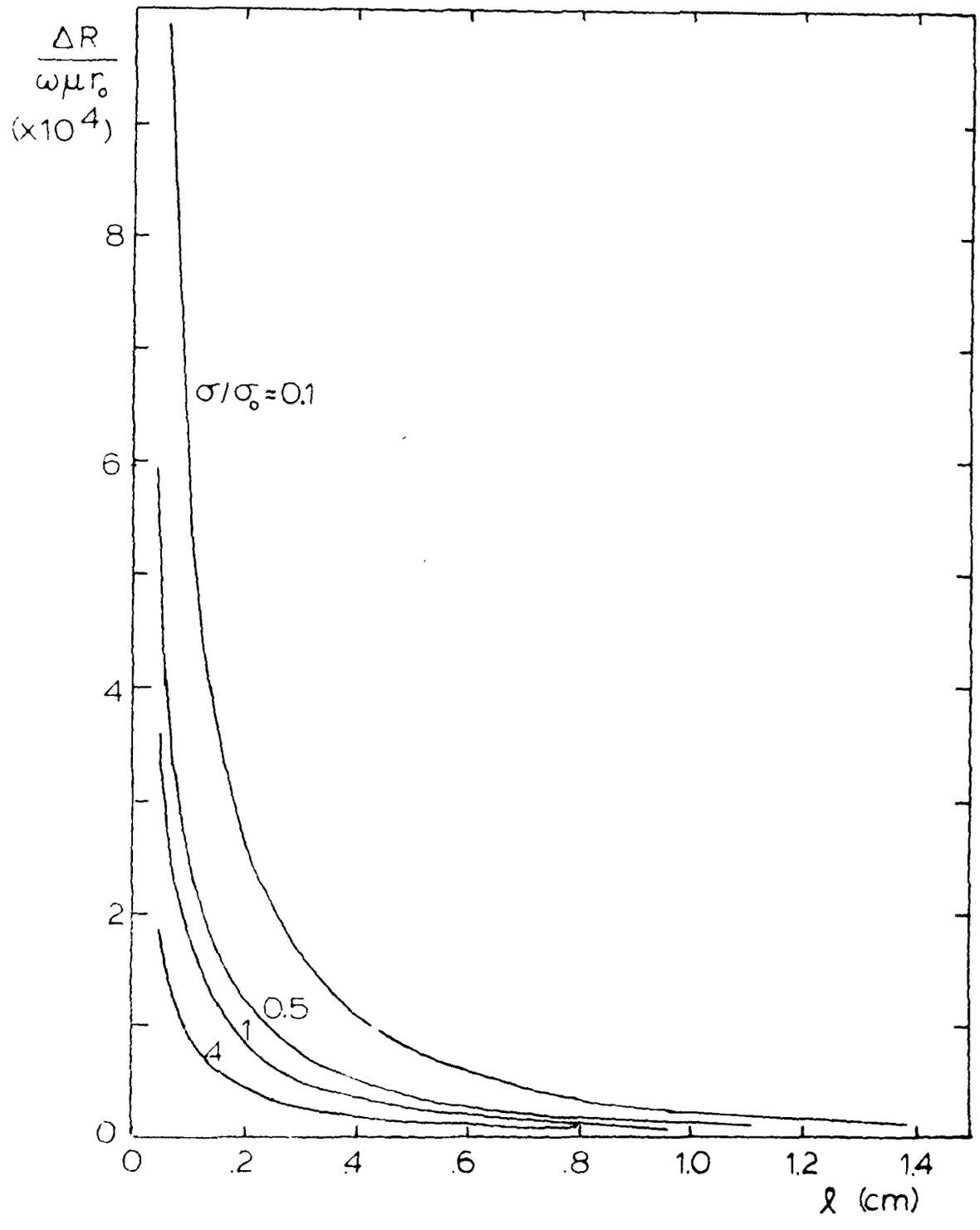
ΔR / ωμr₀ (×10⁴)
8
6
4
2
0
σ/σ₀ = 0.1
0.5
1
4
0
.2
.4
.6
.8
1.0
1.2
1.4
ℓ (cm)

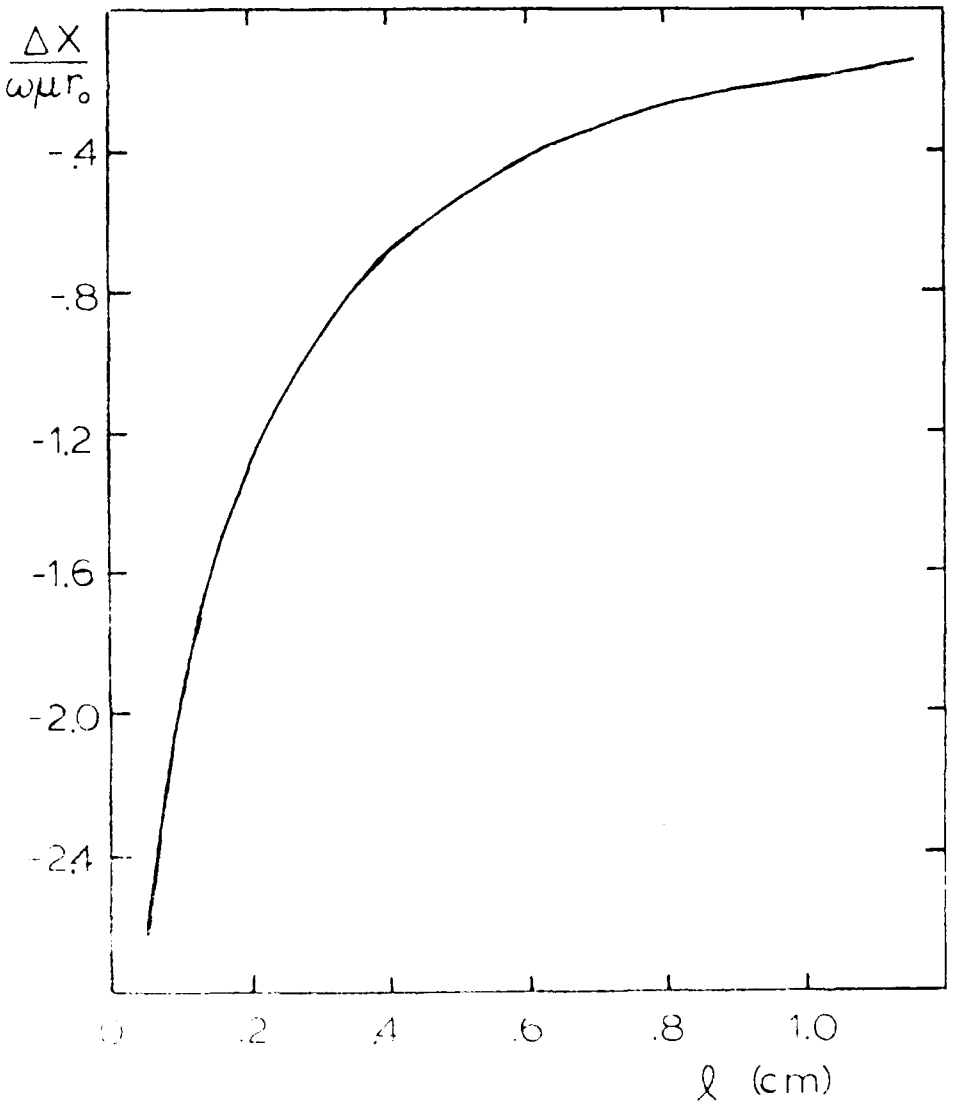
ΔX / ωμr₀
-.4
-.8
-1.2
-1.6
-2.0
-2.4
0
.2
.4
.6
.8
1.0
ℓ (cm)

AD-A084 242 CULLEN COLL OF ENGINEERING HOUSTON TEX F/G 14/2
INTERDISCIPLINARY STUDY ON ADVANCED NDI TECHNIQUES.(U)
JAN 80 A B EL-KAREH, S LONG, C G GARDNER AFOSR-77-3457
UNCLASSIFIED AFOSR -TR-80-0331 NL

2 OF 2
AD
A084242

END
DATE FILMED
6-80
DTIC

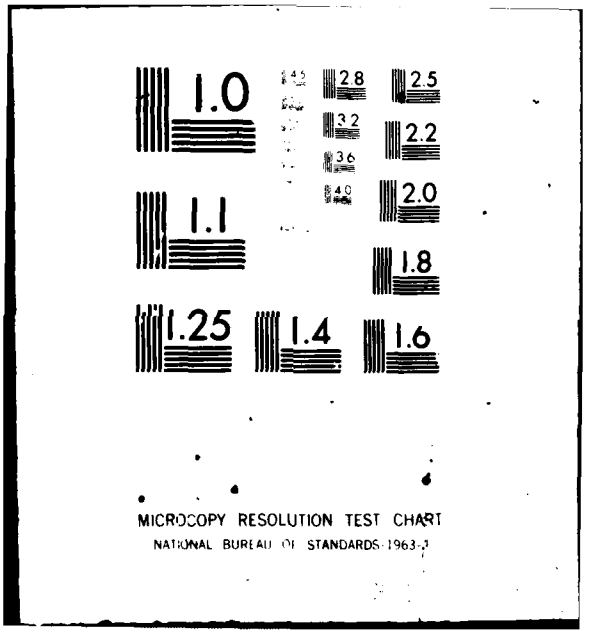
1.0
2.8
2.5
3.2
2.2
3.6
4.0
2.0
1.1
1.8
1.25
1.4
1.6
MICROCOPY RESOLUTION TEST CHART
NATIONAL BUREAU OF STANDARDS-1963-A

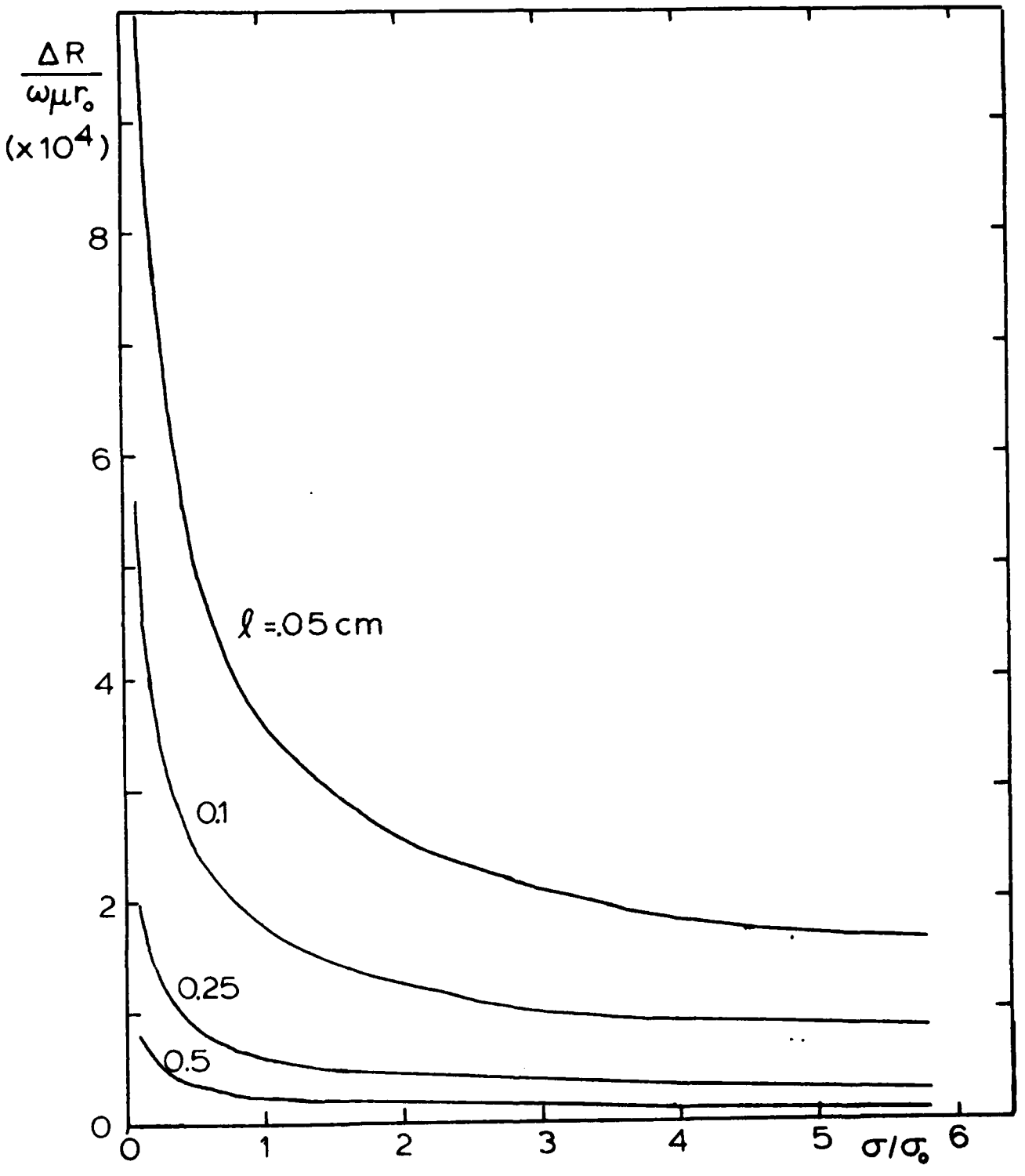
ΔR / ωμr₀ (x10⁴)
8
6
4
2
0
ℓ =.05 cm
0.1
0.25
0.5
0
1
2
3
4
5
6
σ/σ₀

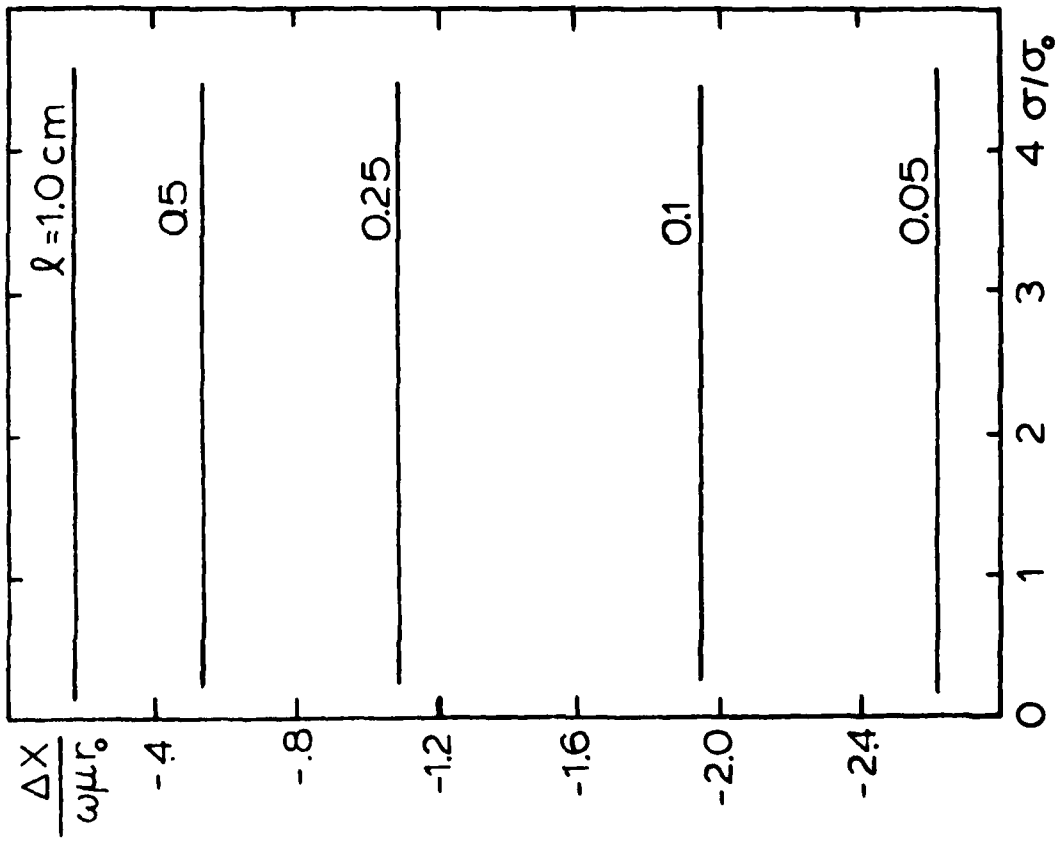
$\frac{\Delta X}{\omega \mu r_o}$
-.4
-.8
-1.2
-1.6
-2.0
-2.4
0
1
2
3
4 σ/σ_o
ℓ =1.0 cm
0.5
0.25
0.1
0.05

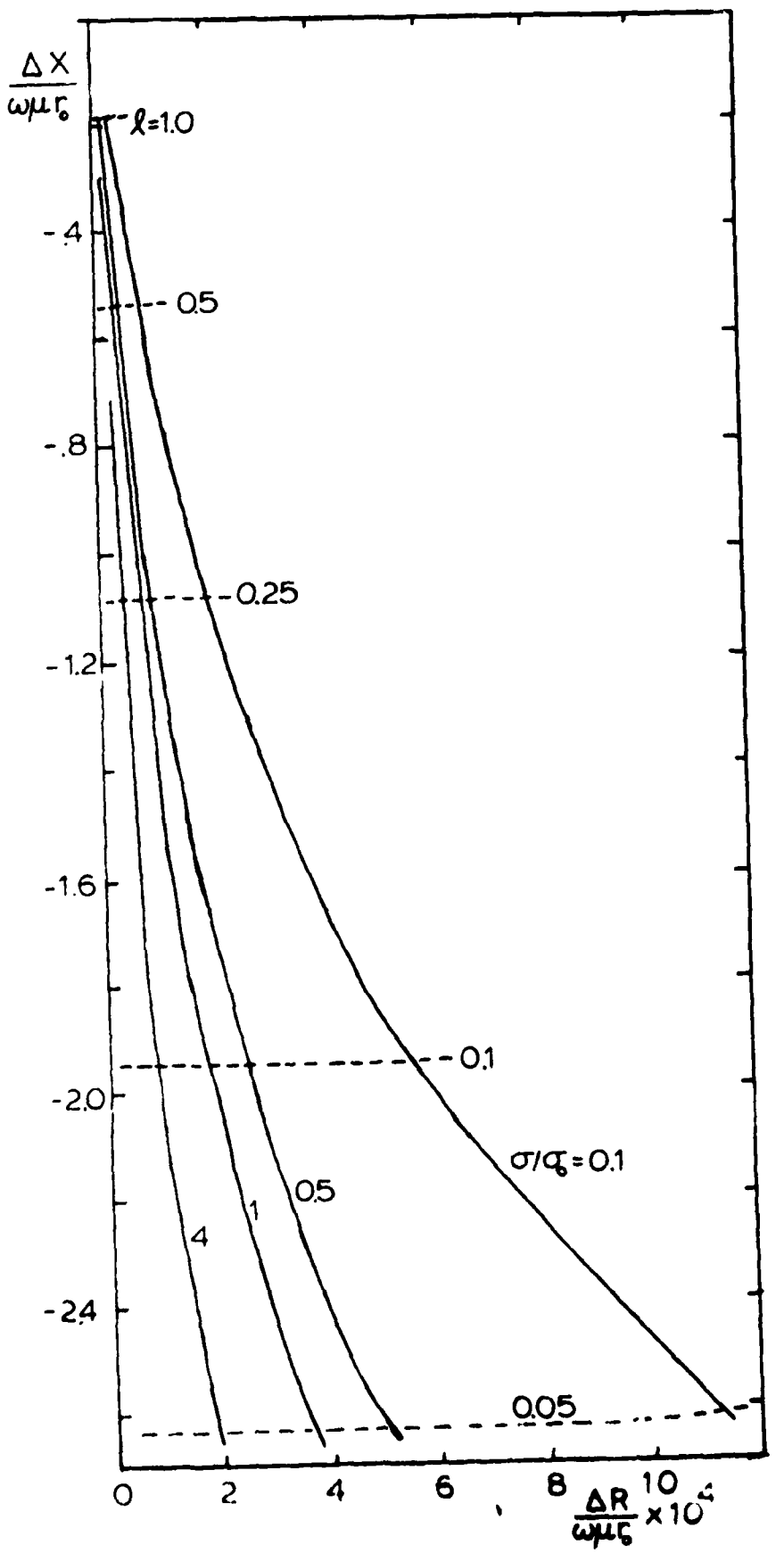
ΔX / ωμr₀
ℓ=1.0
-.4
0.5
-.8
0.25
-1.2
-1.6
0.1
-2.0
σ/σ₀=0.1
0.5
1
4
-2.4
0.05
0
2
4
6
8
10
ΔR / ωμσ₀ × 10⁴